PCCP

ROYAL SOCIETY OF CHEMISTRY

PERSPECTIVE

View Article Online
View Journal | View Issue



Cite this: *Phys. Chem. Chem. Phys.*, 2023, **25**, 24244

# From materials to clinical use: advances in 3D-printed scaffolds for cartilage tissue engineering

Hewen Zhang,†[abe] Meng Wang,†[c] Rui Wu,†[d] Jianjun Guo,[e] Aihua Sun,[e] Zhixiang Li,[e] Ruqing Ye,*[c] Gaojie Xu[e] and Yuchuan Cheng *[be]

Received 28th February 2023,
Accepted 19th August 2023

DOI: 10.1039/d3cp00921a

rsc.li/pccp

Osteoarthritis caused by articular cartilage defects is a particularly common orthopedic disease that can involve the entire joint, causing great pain to its sufferers. A global patient population of approximately 250 million people has an increasing demand for new therapies with excellent results, and tissue engineering scaffolds have been proposed as a potential strategy for the repair and reconstruction of cartilage defects. The precise control and high flexibility of 3D printing provide a platform for subversive innovation. In this perspective, cartilage tissue engineering (CTE) scaffolds manufactured using different biomaterials are summarized from the perspective of 3D printing strategies, the bionic structure strategies and special functional designs are classified and discussed, and the advantages and limitations of these CTE scaffold preparation strategies are analyzed in detail. Finally, the application prospect and challenges of 3D printed CTE scaffolds are discussed, providing enlightening insights for their current research.



## 1. Introduction

Human cartilage tissue is essential for supporting and moving joints. The major components of cartilage tissues are chondrocytes, matrices, and fibers. Articular cartilage (AC) is a form of hyaline cartilage with a lot of matrix and little collagen fiber. It is often described as a smooth, avascular connective tissue that is 2–7 mm thick and covers the surface of the joint.[1,2] Its main job is to lubricate joint motion and absorb shock from cyclic compression stresses when the joint moves.[3] It does, however, have a limited capacity to heal itself, just like the majority of human tissues and organs. Therefore, injuries, mishaps, and tissue lesions frequently result in a great deal of problems for people over time.[4] The whole joint, including the articular cartilage, subchondral bone, ligaments, and other tissues is affected by osteoarthritis (OA), a common degenerative joint condition that results in cartilage abnormalities (when OA occurs, the articular cartilage is severely thin or lost, the subchondral bone is sclerotic, and the articular capsule becomes thickened[5–7]). A vicious loop exists between the deterioration of OA and the imbalance of cartilage deterioration/repair. More than 22.7 million individuals globally currently are affected by OA, which has annual economic impacts in billions in terms of medical expenses and lost wages.[8] Over the following ten years, this number is expected to increase by almost 50%. Therefore, the fundamental objective of treating OA is to restore cartilage tissue defects, and this need is now urgent.

Articular cartilage tissue is composed of a compositionally differentiated extracellular matrix (ECM) constructed by chondrocytes, whose main components include water (about 70%), a type II collagen crosslinking network, and protease. As shown in Fig. 1, articular cartilage tissue can be spatially divided into four layers. The outermost layer is the superficial zone, where the long axis of the flattened oval chondrocytes is parallel to the surface of the cartilage, the collagen fibers are dense,[6] and the structure and integrity of the superficial zone affect the tensile load performance of the articular cartilage.[9,10] Next, the middle zone (transition zone) is adjacent to the superficial zone, which accounts for 40–60% of the total cartilage thickness and isotropically oriented collagen fibers are dispersed to better absorb compression forces.[11,12] Further down, it reaches the deep zone, where chondrocytes mature, increase in size, and

[a] *School of the Faculty of Mechanical Engineering and Mechanic, Ningbo University, Ningbo, Zhejiang Province, 315211, China*
[b] *Center of Materials Science and Optoelectronics Engineering, University of Chinese Academy of Sciences, Beijing 100049, P. R. China*
[c] *Department of Joint Surgery, The Affiliated Hospital of Medical School of Ningbo University, Ningbo, 315020, China. E-mail: yeruqing630149@126.com*
[d] *Department of Orthopedics, Ningbo First Hospital Longshan Hospital Medical and Health Group, Ningbo 315201, P. R. China*
[e] *Zhejiang Key Laboratory of Additive Manufacturing Materials, Ningbo Institute of Materials Technology & Engineering, Chinese Academy of Sciences, Ningbo 315201, P. R. China. E-mail: yccheng@nimte.ac.cn*
† These authors contributed equally to this work.

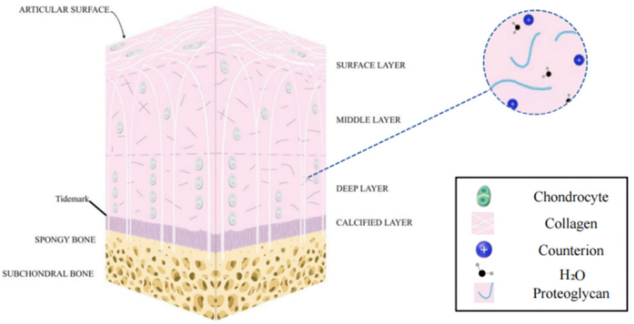


Fig. 1 A schematic diagram of the multi-layered structure of articular cartilage[2] (Copyright © 2022, The Author(s). Published by Elsevier Ltd).

appear elliptical or circular.[6] Collagen fibers are arranged parallel and perpendicular to the surface of the cartilage, increasing compression resistance.[13] A thin layer named tide mark (2–5 μm)[14,15] can be observed between the deep zone (radial zone) and the calcified zone located in the deepest regions. The calcified zone interacts closely with the subcartilaginous bone, allowing the articular cartilage to anchor strongly to the subcartilaginous bone, while facilitating the transfer of transient stress from the articular cartilage to the bone.[16]

Articular cartilage is typically subjected to physical compressive stress between 0.5 MPa and 7.7 MPa, depending on the interaction between multiple substances within the ECM (*e.g.* extracellular collagen and aggregating glue networks).[7,17,18] Ideally, scaffolds should replace the ECM, thereby providing structural support for cell migration, tissue formation and remodeling.[19–21] This functionality is largely dependent on adequate mechanical and biological scaffold properties.[22–24] Therefore, imitation and reconstruction of multi-layered cartilaginous ECM is a key issue for cartilaginous repair.[25]

At the clinical level, several methods have been explored for cartilage restoration, such as cell therapy, osteochondral grafting (OCG),[26] microfracture techniques,[6,27,28] osteochondral autograft transplantation,[29] and autologous chondrocyte implantation (ACI).[30–33] Unfortunately, most of these strategies have poor biological compatibility, poor mimicry of natural tissues (the reconstructed cartilage tissue is less durable than hyaline cartilage and more prone to re-injury[34]), and susceptibility to immune rejection and other complications.[35] All of these factors greatly limit the use of these treatments.

Tissue engineering (TE) is an emerging interdisciplinary field that combines the use of cells, biomaterials, and bioactive factors (or bioreactors) to develop biological alternatives that regenerate, maintain or improve tissue function.[36] The advancement of tissue engineering opens up new avenues for the clinical treatment of skin,[37] liver,[38] and cardiovascular[39] and musculoskeletal tissues.[40] A TE scaffold, an important part of regenerative medicine, can imitate the microenvironment, structure, and function of natural tissues,[14] and provides a physical support for cell aggregation and infiltration[41] and offers a physicochemical environment conducive to successful tissue regeneration.[42] Suitable cells can be attached to the scaffolds, cultured *in vitro* for a period of time, and then implanted inside the body. Typically, TE scaffolds have a three-dimensional (3D) interconnected pore structure, which gradually degrades and is replaced by new tissues in the human body. Biomaterial-based scaffolds can also be combined with suitable growth factors and excellent biomimetic structures to further promote tissue regeneration. Therefore, the manufacturing of TE scaffolds requires flexible and high-precision processing.

3D printing, also known as additive manufacturing, was first proposed by Hull's team in 1987. Based on a digital model created by computer-aided design, a real and physical 3D entity is obtained by accurately and rapidly accumulating materials layer by layer[43,44] using various types of 3D printers and computer-aided manufacturing. 3D printing technology provides powerful engineering design options for biomedicine-related complex devices, such as drug printing, medical diagnostic models, biosensors, tissue engineering, and artificial organs. The emergence of 3D printing technology facilitates free fabrication of a variety of complex biologically inspired 3D structures and brings new ideas for customizing high-performance and multifunctional scaffolds.

With the development of 3D printing over the last ten years, an increasing number of research studies on tissue engineering scaffolds have reported this processing approach, and the number of papers has been increasing. Fig. 2 displays data for articles extracted from Web of Science for a ten-year period

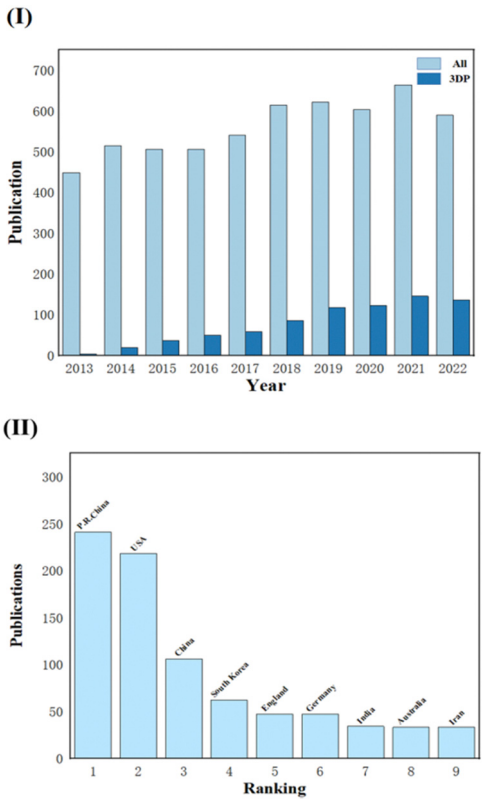


Fig. 2 The statistical data of publications on the topic of CTE scaffolds from Web of Science. (I) Quantitative comparison between all preparation strategies and 3DP strategies under the CTES topic, (II) publications in different nations/regions.

(2013–2022). When looking for the topic CTES, the number of all relevant studies (All) compared to studies involving 3D printing (3DP) is displayed in Fig. 2(I). The latter is growing yearly, and it is obvious that TE professionals are paying more attention to this technology. Fig. 2(II) also displays the quantity of pertinent research conducted in various countries and areas at the same period. We can see that academics in China and the United States are quite interested in this subject because a substantial share of study papers comes from these two countries/regions.

Herein, we review the system of materials and printing technology used for 3D-printed CTESs. Firstly, we will summarize the CTESs printed with different materials based on different 3D printing strategies and analyze their advances and defects. Then, excellent biomimetic structural and functional designs from various studies will also be discussed in categories. Finally, in view of the preparation methods used for 3D printed CTES, this paper will discuss their development prospects and several challenges.

## 2. Common methods of 3D printing in tissue engineering

Rapid advances in biomaterials and manufacturing technologies have made possible more high-performance biomimetic CTE scaffolds that mimic the extracellular matrix (ECM) of natural cartilage, in combination with pro-growth factors (such as BMP-2,[45] β-TCP,[46] and others) to promote proliferation and differentiation of attached cells and the production of specific His proteins.[47] 3D printing is an emerging modern processing strategy with high precision and flexibility. In recent years, the combination of the biomimetic tissue reconstruction concept and 3D printing has led to a new strategy for 3D bioprinting, which has been rapidly used in the field of TE to reinvigorate the design and manufacture of TE scaffolds. Using materials including biomaterials, bioactivators, and even cells, 3D bioprinting takes advantage of 3D printing to create structures close to the body's natural tissues.[48] Table 1 records CTE scaffolds made using different 3D printing methods and their mechanical properties are quantified in it.

As shown in Fig. 3, depending on the printing principle, 3D bioprinting can be classified into the following categories: direct ink writing (DIW), stereolithography (SLA), selective laser sintering (SLS), fused deposition modeling (FDM), *etc.* A wide variety of biomaterials have been applied in different forms in these 3D printing strategies. This section discusses in detail these 3D bioprinting strategies and potential applications of biomaterials in 3D bioprinting to create engineered scaffolds for cartilage tissues.[68]

### 2.1. Direct ink writing

The most prevalent type of 3D bioprinting is extrusion-based and it mostly uses mechanical and pneumatic extrusions. DIW is a typical extrusion-based technology. Bio-inks are pressurized or mechanically driven by matching nozzles for viscoelasticity (loss modulus $G''$ and storage modulus $G'$). The bio-ink probed here is usually a non-Newtonian fluid whose viscosity decreases as the shear rate increases and returns to its original state after the shear forces disappear. In addition, bio-inks have low surface tension and adhesion and their particles distribute uniformly and flow without adhering to the nozzle. To alter

Table 1 CTE scaffolds made using different 3D printing methods and their mechanical properties

| Processing strategies | Processed materials | Mechanical properties of scaffolds | Ref. |
|---|---|---|---|
| Direct ink writing | Alg/PCL/PLA/PLGA | Compressive modulus ($E'$): 15.31 MPa | 49 |
| | Alg/Gel/HA/CPCs/FN | Compressive modulus ($E'$): 11.20 ± 0.40 kPa | 50 |
| | Alg/NC/Chs/DS | Compressive modulus ($E'$): ∼0.20 kPa | 51 |
| | Alg/nHA/CS | Compressive modulus ($E'$): ∼300 kPa | 52 |
| | PLGA | Biomechanics of the regenerated area: ∼45 N | 53 |
| | PCL/GelMA/DCECM | Compressive modulus ($E'$): 24.62 ± 8.89 MPa | 54 |
| | Alg/PEG | Compressive modulus ($E'$): 4.43 ± 0.21 MPa | 55 |
| | PGD/APGD | Tensile modulus ($E$): ∼5 MPa, tensile strength: ∼1.2 MPa | 56 |
| | PU/HA | Compressive modulus ($E'$): 0.33 ± 0.02 MPa | 57 |
| | PU | Compressive modulus ($E'$): 0.94 ± 0.01 MPa | 58 |
| Stereolithography | PEG-DA/PLGA/nHA | Compressive modulus ($E'$): ∼12 MPa, compressive strength: ∼25 Mpa | 59 |
| | NARMA/GELMA | Compressive modulus ($E'$): ∼40 KPa, compressive strength: ∼27 Kpa | 60 |
| | GelMA/PTMC | Tensile modulus ($E$): 4.62 ± 0.84 MPa, tensile strength: 0.52 ± 0.18 Mpa | 61 |
| Selective laser sintering | PCL/nHA | Compressive modulus ($E'$): 8.7 MPa, compressive strength: 4.6 Mpa | 62 |
| | PCL | Compressive modulus ($E'$): 5.91 MPa (consecutive-channel scaffold) | 63 |
| Fused deposition modeling | PLA/ABS | Compressive modulus ($E'$): ABS ∼200 KPa, PLA ∼600 KPa | 64 |
| | Alg/ALG-SUL/dECM/PCL | Compressive modulus ($E'$): 0.27 ± 0.04 MPa, compressive strength: 6.26 ± 0.27 MPa | 65 |
| | Insulin-PLGA/PDA/PCL | Compressive strength: 6.21 ± 0.63 MPa, compressive modulus ($E'$): 233.71 ± 7.57 MPa (maximum) | 66 |
| | PCL/PLA/nHA | Compressive modulus ($E'$): 1.01 ± 0.04 GPa (blank), 1.07 ± 0.16 GPa (nHA); compressive strength: 77.92 ± 2.4 MPa (blank), 83.19 ± 1.63 MPa (nHA); tensile modulus ($E$): 1.10 ± 0.03 GPa (blank), 0.97 ± 0.11 GPa (nHA); and tensile strength: 64.29 ± 3.64 MPa (blank), 52.91 ± 1.73 MPa (nHA) | 67 |

 

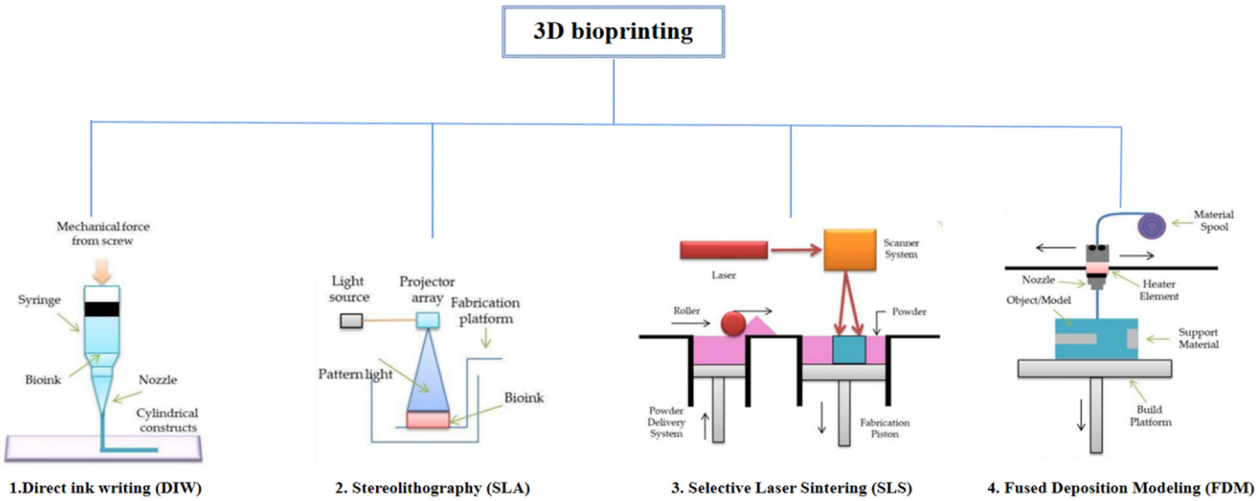


Fig. 3 Classification of 3D printing technology depending on the principle of 3D printing[69] (Copyright © 2021, MDPI).

the precision and speed of printing, the nozzle size and print settings (extrusion speed and printing speed) were varied. Smaller nozzles can achieve a 3D structure with higher print resolution and less tolerance for shape at a lower printing speed, but also greatly lengthen the manufacturing cycle. Based on its rheological characteristics, ink solidifies either naturally or artificially after leaving the nozzle. In order to maintain shape fidelity, the material is changed from a shear-thinning fluid to a viscoelastic solid in natural curing. The $G'/G''$ ratio can be used to quantify the properties of the inks discussed above (with the ratio $>1$, the ink becomes solidified; with the ratio $<1$, the ink becomes semi-solid or gelatinous). When deposited on a substrate, artificial curing strategies such as photocrosslinking, solvent evaporation, and heat treatment temperature-driven reactions can be used.[70,71]

Direct ink printing has the advantages of being inexpensive, straightforward operation, and highly material compatible, and has the capacity to combine multiple materials. Fig. 4 shows some of the related studies carried out on the use of suitable natural and synthetic biological materials in the realm of medicine.

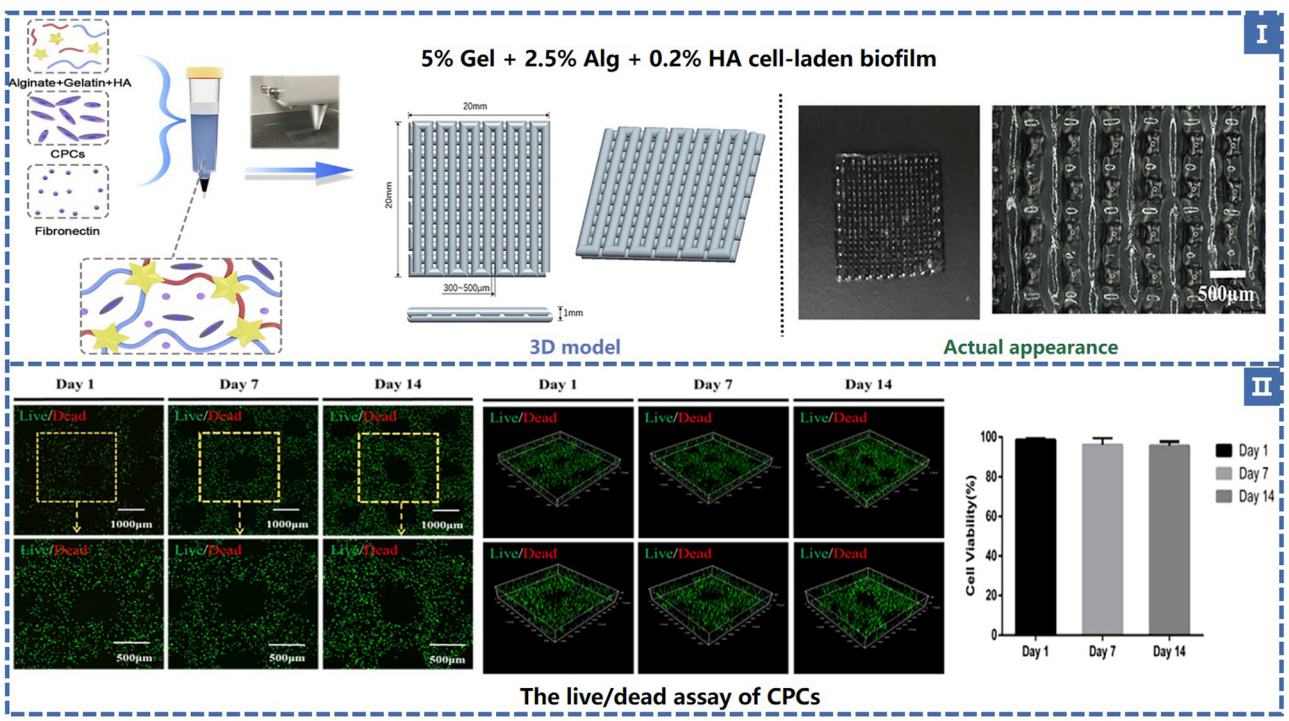


Fig. 4 (I) TE scaffold composition and geometry. (II) The live/dead assay of CPCs and the cell viability in 14 days[50] (Copyright © 2021, The Authors. Published by Elsevier Ltd.).

### 2.2. Stereolithography

As the most accurate and earliest practical rapid prototyping technology in 3D printing, stereolithography uses a computer to accurately control the movement of a laser beam and liftable platform, solidifying liquid photosensitive materials layer by layer along the designed scanning path in accordance with a pre-sliced 3D model to complete the creation of a solid. In general, UV or visible light irradiation of photoinitiators in liquid photosensitive materials is chosen to promote curing.[72,73] The structure size in the $x$ and $y$ directions depends on the spot size of a laser generator, which can guarantee the high resolution of printing.[74,75] While most commercial printers have a maximum accuracy of 50–200 microns, SLA printers can even achieve ultra-high accuracy of up to 20 microns. According to the movement method of the mobile platform, SLA may be further separated into top-down and bottom-up.

The laser light source of the former is placed above the material groove. When a layer of scanning and curing is completed, the printing platform will move down one layer of height, so it is called sunken stereolithography. This method of printing has a problem: the depth of the forming height size and material slot are closely related, and the user needs to fill in the slot at least theoretically and print the same depth of liquid photosensitive material structure height, which makes use of a greater amount of raw materials than that required for printing the finished product, causing a lot of waste. Pull-on SLA improved this problem very well, its scan light source is located in the material tank below, each layer of the curing also occurs on the photosensitive material exposed to air, then the platform at the same height moves up away from the contact surface, liquid materials, relying on gravity flow to fill the gap, and the ultimate finished product will be placed down on a mobile platform for printing. The latter achieves a larger print size with a smaller volume, saves material costs, and improves printing efficiency; therefore, it can be better promoted for desktop-level printing equipment.

SLA is a nozzle-free, jet-free printing method, its bio-inks have a wide range of viscosity options (1–300 Mpa s) and avoids shear stress on bio-inks (liquid photosensitive materials), ensuring high bioactivity.[76] To further pursue the resolution and efficiency of printing, a disruptive digital light processing technology (DLP) similar to SLA has entered the public spotlight. An original laser generator that can transmit light beams has been replaced with a digital micro-mirror lens, and it can scan a two-dimensional plane. The realization of a higher resolution (about 1 um size of the geometric shape) based on the projection form one-plane printing greatly shortens the manufacturing cycle. While SLA (or DLP) offers numerous advantages, there are also limitations associated with printing materials: liquid photosensitive materials must contain specific reactive groups to allow cross-linking and curing with photoinitiators; At the same time, the materials need to be transparent with limited scattering so that the scanning light can pass evenly. A significant number of scaffolds based on SLA/DLP approaches have been described in the investigation of CTE, despite the fact that there are several difficulties in this approach.

### 2.3. Selective laser sintering

Selective laser sintering involves the laser irradiation of high temperature melting sintering accumulation while using powdered or granular materials. It realizes accurate positioning and scanning through a computer controlled light source positioning device. After completing the curing of one layer of material, the surface of the curing layer will be covered with another layer of raw materials to continue printing. No support required, simple operation, and fast printing speed are the significant advantages of this printing method. However, the high temperature produced by laser heating easily leads to the degradation of biological materials, and the introduction of bioactive substances before the whole printing process becomes a tricky problem. At the same time, the surface of the structure printed using this method is relatively rough and requires post-treatment. Currently, SLS is commonly utilized to fabricate metal, bioceramics and some engineering plastic scaffolds, but printing hydrogels is not feasible for the time being. This technique has relatively low requirements for printing materials. The powders (or particles) needed for sintering must possess a specific particle size (usually in the range of a few microns to several hundred microns[77]) and be in a good spherical state,[77,78] since both will have an immediate impact on the material's mobility in the powder bed. Because of the direct relationship between material fluidity and SLS printing, it is essential to guarantee that the powder can be compactly and evenly dispersed over the plane at high temperatures. Moreover, the consolidation phenomenon of polymers is still rarely described in the literature,[79] which eventually leads to the problem of a few types of SLS powders for commercial use.

### 2.4. Fused deposition modeling

Fused deposition modeling technology is the most mature and widely used additive manufacturing technology. The printer based on this technology has the advantages of a simple structure, easy operation, a low material loss rate, and a low maintenance cost. In the process of FDM printing, thermoplastic engineering plastics in the form of wire are fed into the wire feeding mechanism and pushed into the nozzle. The thermoplastic quickly melts into a semi-liquid after being heated at a high temperature, is extruded, and is then deposited on the workbench. After cooling, the shape is fixed as the section shape of the model in this layer and finally, the 3D workpiece is completed by stacking layer by layer. The precision of this printing method is affected by the extrusion pressure and the diameter of the extrusion needle. The printing speed is limited by the melting viscosity of the material, the environment, and the temperature of the nozzle, and is relatively slow. To prevent collapsing, some complex spatial structures also need to be supported.

There are many kinds of thermoplastic engineering plastic wire suitable for the FDM method, such as butadiene–styrene (ABS), polyvinyl alcohol (PVA), polyurethane (TPU), and polylactic acid (PLA). The number of studies on PLA and PCL is relatively high in the field of CTE.

# 3. The biomaterial selection for 3D-printed CTE scaffolds

## 3.1. Natural polymers

The most typical natural polymer materials utilized in 3D-printed CTE scaffolds are hydrogels because their polymer networks can accommodate large amounts of water. They mimic the composition and structure of the natural cartilage ECM to a certain extent,[80,81] creating a physicochemical microenvironment suitable for the proliferation and differentiation of mesenchymal stem cells, but are constrained by their weak mechanical properties (even an order of magnitude less than cartilage), which makes scaffolds difficult to mimic cartilage. Natural polymers that have attracted much attention in academia include gelatin, silk fibroin,[82] alginate, hyaluronic acid,[83] chondroitin sulfate, chitosan,[84] *etc.* To build CTE scaffolds, extrusion-based bioprinting employs one or more of these materials.

Gelatin is essentially a peptide mixture obtained by partial hydrolysis of type I collagen,[85] which is excellent due to its biocompatibility, degradability, and accessibility.[86] Huang *et al.* reported a gelatin scaffold doped with hydroxyapatite (HAP) based on extruded bioprinting.[87] They prepared a HAP scaffold out of 10% gelatin and 5% volumetric weight, then soaked it in 1% (w/v) streptococcal transglutaminase for 6 hours to cross-link it. The resulting scaffold porosity was $81.29 \pm 2.05\%$, water content was $84.29 \pm 0.75\%$, and human umbilical cord blood-derived mesenchymal stem cells (hUCB-MSCs) adhered, migrated, and proliferated well within this scaffold.[87] Their work demonstrated a strategy to modulate the fluidity of gelatin by doping nano-hydroxyapatite (HAP), which could fine-tune the fluidity and gelation time to optimize the rheological properties of gelatin; HAP insertion into gelatin scaffolds, however, significantly improved MSC differentiation and cartilage repair effectiveness, while marginally reducing cell survival and proliferation rates *in vitro*.

Huang *et al.* demonstrated the application of DLP printing technology in the field of cartilage repair scaffolds.[60] They discovered that naringin (NAR), a natural flavonoid found in citrus plants, has great potential for application in knee rehabilitation.[88,89] Methacrylic anhydride (MA) was used as the matrix, NAR was used a modified substance to synthesize NARMA, and a little amount of GELMA was employed as an excipient to obtain a NAR-derived bioink (NARMA-GelMA bioink) with photo cross-linking, high fidelity and good mechanical properties. The bio-ink was used to print (DLP) loop structures with intersections and compared them with the same structures constructed using GELMA. NAR derived bioinks are more resistant to light scattering, enhancing optical cross-linking performance of the MA based ink, ensuring print fidelity. At the same time, it retains high bioactivity in cell culture experiments. When the transcription of SoX9 gene was measured using the RT-qPCR method, it was found that the addition of NAR highly promoted the chondrocyte phenotype and was suitable for 3D bioprinting to form a new cartilage tissue ink.

Silk fibroin (SF) is a natural protein material derived from the secretions of the silkworm, spider, bee, and other animals. It has a complicated molecular structure made up of light chains (26 kDa) and heavy chains (390 kDa), which are joined together by disulfide bonds.[90] Silk fibroin has been effectively used in clinical practice by being formed into surgical sutures, artificial blood vessels, and wound dressings due to its superior mechanical qualities, great biocompatibility, excellent degradability, and numerous supplies.[91] Weili Shi *et al.* manufactured an SFG-E7 scaffold with dual structural and functional optimization through DIW technology.[92] Gelatin and silk fibroin were blended in a mass ratio of 1 : 1 (6.9% w/v) and the E7 peptide was then added to balance the mechanical qualities and degradation rate. A uniform pore size of 350 um was designed to promote the proliferation, differentiation, and ECM production of BMSCs. This doubly optimized scaffold exhibits improved efficacy in knee cartilage regeneration because it not only attracts and maintains enough BMSCs but also offers mechanical protection before the development of new cartilage and an appropriate 3D microenvironment for BMSCs.

Alginate (Alg) is a polysaccharide carbohydrate extracted from brown algae. Low price, easy availability, good biocompatibility and low immunogenicity are the advantages of this natural polymer material, so it is widely applied in the biomedical field[93] as medical swabs, dental impression materials, surgical dressings, *etc.* Alginate has the capacity for fast gelation when combined with divalent cations, such as $Ca^{2+}$.[94] Alginate saline gel is one of the bioinks commonly used in extruded bioprinting. Susan Critchley *et al.* prepared a variety of fiber reinforced sodium alginate hydrogel CTE scaffolds using PCL, PLGA and other materials for printing network structures as mechanical supports (as shown in Fig. 7).[49] Among them, sodium alginate hydrogel has been used as an excellent carrier to carry bioactive materials such as BMSCs and chondrocytes. Of course, alginate can also be combined with other substances to create composite hydrogel bioinks that can be printed directly into the porous scaffold's body. He *et al.* made a composite hydrogel (Alg/Gel/HA) using alginate, gelatin, and hyaluronic acid, and the cartilage progenitor cells (CPC) and fibronectin (FN) were also encapsulated in the bio-ink. CPCs achieved separation, migration, and proliferation through differential adhesion on FN (Fig. 4).[50] Finally, chondrogenesis is accomplished.[95] The generated 3D printed bioactive biofilm (1 mm thick scaffold) was made to modify the AMIC technique (autologous matrix-induced chondrogenesis technique is a one-step procedure for healing cartilage defects, a fibrin membrane or collagen membrane will be implanted in the defect[6]), which replaced the traditional collagen membrane and covered the tissue defect site, providing sufficient mechanical support and structural integrity to provide a stable microenvironment for BMSC released from the subchondral bone. This approach effectively improved the thickness and quality of the newly generated cartilage, significantly enhanced the results of AMCI, and was more conducive to clinical translation.

Hyaluronic acid (HA) is an acidic glycosaminoglycan composed of two disaccharide units, D-glucuronic acid and

*N*-acetylglucosamine. Its molecular weight is generally in millions and its content is high in brain nerve tissue, connective tissue, and epithelial cells. As a component of chondrocyte extracellular matrix and synovial fluid, hyaluronic acid has the functions of joint lubrication, wound healing, and strong water retention. In addition, the inclusion of the methacrylate group gives hyaluronic acid the ability to light-cure,[96] classifying it as one of the raw components for bio-ink. At present, a hyaluronic acid-based cartilage repair scaffold (Hyaff-11) has been commercially produced in Italy. This scaffold has time-controlled characteristics. Compared with chondrocyte transplantation without *in vivo* fixation, it exhibits excellent biocompatibility and the capacity to reconstruct cartilage.[6,97] Autologous chondrocyte transplantation using Hyaff-11 significantly improved the repair capacity of articular cartilage according to histological and histomorphological analysis. After 24 weeks, hyaline cartilage prevailed at the original defect. These cartilage sites had a well-organized histoarchitecture and columnarisation, and ECM formation was observed. (In the control group in which the cartilage defect was not treated with Hyaff-11, no signs of extracellular matrix formation were observed after 24 weeks.)

Chondroitin sulfate (ChS) is a sulfated glycosaminoglycan composed of *N*-acetylgalactosamine and glucuronic acid (GAG, the previously mentioned HA is a non-sulfated glycosaminoglycan). As one of the important components of cartilage, chondroitin sulfate attaches to proteins to form proteoglycans, endowing cartilage with strong compressive resistance and providing mechanical protection.[94] At the same time, it has also been reported to promote cell differentiation,[98] improve anti-inflammatory activity,[99] and aid cartilage recovery,[100] and has been manufactured as a dietary supplement, forming a method to improve and even treat osteoarthritis (OA).[6,99] Markel Lafuente-Merchan *et al.* added chondroitin sulfate to nanocellulose alginate saline gel to improve the rheological properties of bio-ink and improve the resolution and shape fidelity of scaffold printing: The viscosity of bio-inks increased somewhat with the addition of ChS. However, when the shear rate increased, they also displayed a shear thinning behavior and as the shear rate reverted to its initial level, the viscosity was recovered. This contributes to the fidelity of the scaffold's shape after printing. Cell survival and chondrogenic differentiation capacity were dramatically increased when ChS was added compared to the blank control group (without ChS) (as shown in Fig. 5).[51] Dermatan sulfate (DS), which is similar to ChS, has also been tried by adding to NC-Alg ink to improve its properties. DS and ChS have the same chemical make-up, however there are certain glucuronic acid residues in DS that go through an epimerization process to become iduronates.[101,102] It can manipulate the behavior of MSCs in terms of adhesion and proliferation. It may also encourage their differentiation[103] and maturation. In terms of rheological qualities (the viscoelasticity of bio-inks), ChS performed better than DS (a higher viscoelastic bio-ink could protect the encapsulated cells from the stress caused by the printing process), but the addition of DS led to greater improvements in cell viability (the live/dead

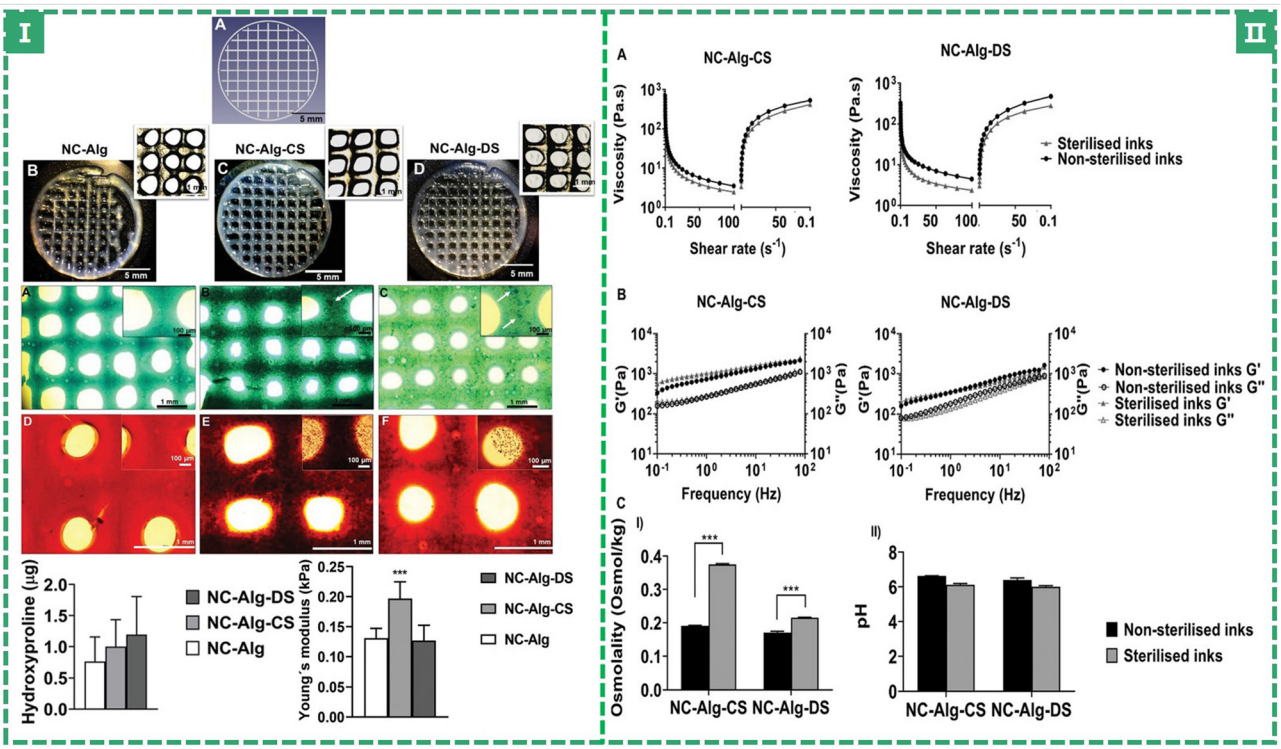


Fig. 5 (I) Printability study and chondrogenic differentiation evaluation of bioprinted scaffolds. (II) Evaluation of the sterilisation procedure on NC-Alg-CS and NC-Alg-DS inks' properties.[51] (Copyright © 2022. The Authors. Macromolecular Bioscience published by Wiley-VCH GmbH.)

staining: the ChS group showed 80.11 ± 1.85%, but the DS group showed 88.14 ± 2.62% and the blank group showed 77.77 ± 6.80%, a higher percentage means more living cells, which were proliferative and differentiated by MSCs.)

Chitosan (CS) is the structural element of the exoskeleton of crustaceans (such as crabs and shrimps) and the cell wall of fungi in nature. It is a linear polysaccharide composed of two kinds of glucosamine. Chitosan contains glycosaminoglycans that can promote chondrogenesis[104] and has a hydrophilic surface that promotes cell attachment and growth. It is one of the most effective options for CTE scaffold materials due to its superior biodegradeation, antimicrobial, and physiological activity. Huang *et al.* reported in 2014 that their research group prepared hydrogels loaded with BMSCs using chitosan and decalcified bone and they found that it had a significant effect on promoting chondrogenic differentiation.[105] Recently, Ali Sadeghianmaryan *et al.* constructed a novel chitosan/nHA/alginate hybrid scaffold by extrusion bioprinting, making use of an impregnation technique to connect alginate and nano-hydroxyapatite particles (nHA) to the scaffold.[52] Nano-hydroxyapatite particles improve the elastic modulus, thermal stability behavior and cell attachment of scaffolds, and it is beneficial to achieve a stable physical and chemical microenvironment for chondrocytes. The scaffolds impregnated with sodium alginate showed improvement in swelling, hydrophilicity, and cell viability.

### 3.2. Synthetic polymers

Chemical synthesis is also an important source of biomedical polymers. Generally, monomers with known relative molecular mass and material structure are used as raw materials to form polymers through polymerization reactions, such as free radical polymerization, anion/cation polymerization, and coordination polymerization. Synthetic polymers have much improved mechanical properties as compared to natural polymer materials, and scaffolds composed of these materials will have mechanical characteristics more akin to natural cartilage. Common synthetic polymers include polylactide (PLA), polycaprolactone (PCL),[106] polyethylene glycol (PEG),[107] polyglycolic acid (PGA),[108] polyvinyl chloride (PVC), polyethylene (PE), nylon, silicone rubber, poly(1, 3-trimethylcarbonate) (PTMC),[23] polyurethane (PU),[58] *etc.* Researchers have focused primarily on the first two types of artificial polymers in CTE because of their biocompatibility and material degradability.

PLA, also known as poly(lactide), is obtained by dehydration condensation of hydroxyl and carboxyl groups between α-hydroxypropionic acid molecules. It offers high biodegradability, tensile strength, and elongation. It is usually applied in the medical field for producing things like disposable infusion equipment, pharmacologically slow-release packaging agents, and surgical sutures due to its excellent properties. PLA reacts and degrades inside of living organisms before being released as carbon dioxide and water, although this process takes a while—possibly even longer than a year.[19]

Derek *et al.* used the FDM method to print PLA and ABS filaments to obtain an orthogonal scaffold with a pore size of about 700 microns, which is suitable for the growth of chondrocytes and NP (nucleus pulposus, a gelatinous substance in the intervertebral disc) cells and the production of type II collagen and proteoglycans (as shown in Fig. 6).[64] Pariya Zare *et al.* filled alginate sulfate (Alg-Sul) hydrogel into the PCL framework based on FDM printing,[65] which overcame the problem of poor mechanical properties of fiber-reinforced hydrogels reported in previous studies.[109] This composite scaffold not only imitates the mechanical properties of natural nasal cartilage, but also retains the biological similarity between the Alg/ALG-SUL/dECM hybrid hydrogel and human cartilage, demonstrating its great potential for osteochondral repair and regeneration. Pierluca Pitacco *et al.* reported their prepared hMSCs/fibrin bio-ink 3D printing scaffold with a PCL-reinforced skeleton.[110] The PCL skeleton portion was treated with 3 M sodium hydroxide (NaOH) for 12 hours to render the PCL skeleton more hydrophobic and better able to adhere to cell-filled hydrogels.

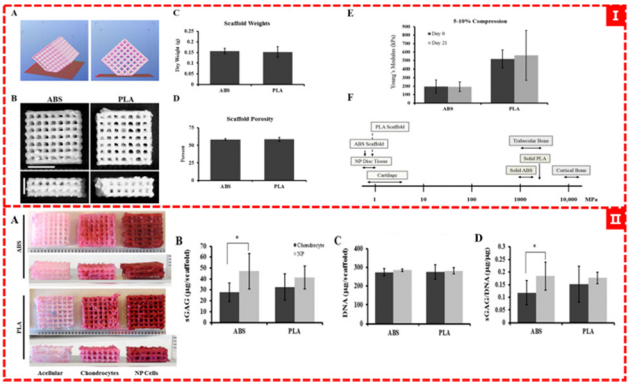


Fig. 6 (I) (A) and (B) ABS and PLA scaffold designs, (C) and (D) quantification of scaffold weight and scaffold porosity, and (E) and (F) mechanical testing of ABS and PLA scaffolds. (II) Proteoglycan analysis of scaffolds[64] (Copyright © 2015, MDPI).

PGA (a saturated fatty acid group polymer) is also a thermoplastic, which can be made into films or scaffolds by extrusion, injection, and hot pressing. The biodegradation cycle of PGA is less than half that of PLA.[6]

In fact, in various studies, monomers (lactic acid and glycolic acid) are used to copolymerize to obtain a better performance of the degradable polymer material, polyethyllactide (PLGA). This substance, which has FDA approval and is listed in pharmacopoeia as a microsphere carrier, and it can be exploited as a pharmaceutical excipient. PLGA degradation products have almost no toxic side effects and do not trigger immunological and rejection reactions in surrounding tissues, which has been continuously studied and reported in the field of TE. Researchers discovered, however, that its breakdown by-products were difficult to eliminate, and lactic acid and glycolic acid accumulated *in situ* to high concentrations, causing the biological response to adversely change when they came into touch with tissues.[20] Peng Chen *et al.* prepared a PLGA scaffold with high biocompatibility and inoculated BM-MSCs overexpressing BMP-12 on the scaffold to evaluate the reconstruction

effect of this method on rotator cuff tissue and fibrocartilage.[53] Collagen organization was enhanced and fibrocartilage deposition was boosted when BMP-12 overexpressed BM-MSC loaded with 3D-printed PLGA scaffolds was applied locally. The degradation of the 3D-printed PLGA scaffold was determined by the weight loss, which reached 75.7% after 12 weeks of incubation in PBS, indicating the scaffold's exceptional degradability.

PLGA microspheres are widely employed as drug delivery vehicles in TE, owing to their capacity to regulate medication release both spacially and temporally. Recently, Peiran Wei *et al.* selected PLGA-coated insulin nanoparticles in order to achieve sustained and delayed drug release. They were then adsorbed on the PCL scaffold's surface to construct a composite scaffold that would release insulin gradually over time, while also continuously inducing osteochondrogenesis.[66] PCL scaffolds were given a biocompatible PDA (polydopamine) modification to provide a thick biofunctional coating that improved hydrophilicity and was beneficial for PLGA nanoparticle (NP) adsorption. The encapsulation efficiency of PLGA NPs for insulin was up to 83.6%, and the cumulative release rate was 88.62% within 30 days. However, the modified insulin-PLGA/PDA/PCL scaffold still maintained a homogeneous and porous microstructure (pore size 418.06 ± 30.17 um and porosity 78.34 ± 3.27%) and excellent mechanical properties (compressive strength 6.01 ± 0.46 MPa). The insulin-PLGA/PDA/PCL scaffold efficiently induced rBMSC differentiation and rabbit chondrocyte proliferation, while enhancing cartilage and subchondral bone healing capacity.

In 2015, Nathan J. Castro *et al.* reported their bionic osteochondral scaffolds printed using tabletop stereo-lithography.[59] The new 3D printing system developed by the team enables rapid fabrication of a photocross-linked hydrogel scaffold, allowing easy modification of the filling density (corresponding to the pore density) and orientation of each corresponding layer of the 3D model, thus ensuring a gradual transition of biological activity and geometry in the structure. They selected two bioactive nanomaterials: hydrothermally treated nanocrystalline hydroxyapatite (nHA) and TGF-β1 coated PLGA nanospheres (SEM image analysis shows that its size range is 75 ± 17 nm). The cartilage portion was simulated with a PEG-Da solution containing PLGA microspheres to which different concentrations of nHA were added to, constructing a gradient subchondral scaffold of bone layers. PEG-Da hydrogel has excellent biological properties and its inherent microporous properties promote the local diffusion of TGF-β1. The hydroheat-treated nHA acts as an exceptional mechanical enhancer in 3D-printed structures that mimic cartilage (nHA increases scafford's performance *via* incorporation within a bulk matrix[21]). Nanospheres not only serve as a continuous drug delivery device, but also inhibit the rapid degradation of low molecular weight PEG to a certain extent and prolong the mechanical support time of scaffolds. Xuan Zhou *et al.* also demonstrated the same type of study in 2019: they added gelatin methacrylate (GelMA) to PEGDA to make a biocompatible primary ink (GelMA-PEGDA);[111] nHA- and TGF-β1-coated PLGA microspheres were mixed based on the primary ink, meanwhile, the biphasic gradient scaffold was printed by stereolithography (SLA) to improve the ability of cartilage repair and osteogenesis.

PCL is a kind of polymer material with a low melting point (59–64 °C) that is made of caprolactone with diol as an initiator. This material offers good biological compatibility, mechanical properties and printability.[6,49,54,106] At the same time, it has been reported to have a certain shape memory (SM) ability,[112] which can be restored from the deformed state to the initial state when the external conditions are appropriately changed. Sutures and drug delivery devices made of PCL have been approved by the FDA. It also has several problems that affect its performance. For instance, the material is hydrophobic, which may prevent the cells from adhering smoothly. The biodegradation cycle of PCL is much longer than that of PLA (2–3 years[113]), *etc.* To overcome these issues, researchers have proposed a variety of modification methods to achieve better cartilage repair outcomes. In the study of Susan Critchley *et al.*[49] mentioned above, a biphase composite scaffold consisting of PCL and alginate was obtained by screw extrusion and printing, and an orthogonal PCL network structure was obtained. MSCs were covered in an alginate saline gel that stimulated cartilage repair by promoting cell adhesion and differentiation. The PCL fiber network serves as a structure for mechanically reinforced alginate saline gels capable of supporting robust cartilage formation (as shown in Fig. 7 and 8). Yang *et al.* reported a bifunctional PCL/GelMA/DCECM scaffold (DPGE) co-printed with the aptamer-GE bioink based on a dual-nozzle bio-printer.[54] PCL has large pores of roughly 800–1000 μm, which serve as the backbone to provide mechanical strength and an anatomical structure for the bifunctional scaffold. In the compressive test, the compressive modulus of the DPGE scaffold is 24.62 ± 8.89 MPa, which can withstand physiological compressive stress,[114] indicating that the introduction of the PCL framework can provide sufficient biomechanical support

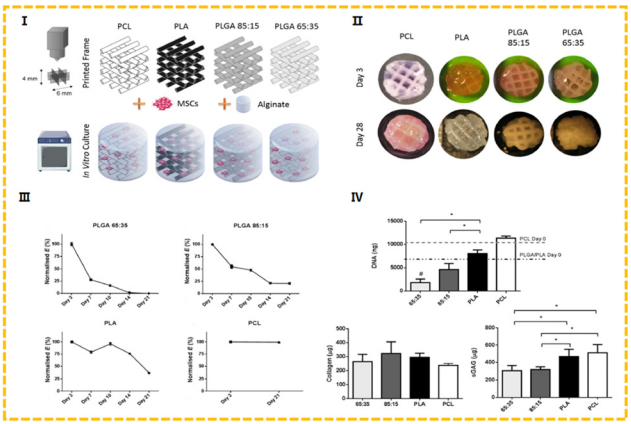


Fig. 7 (I) Outline of the experimental groups, whereby 3D printed polymer frames were combined with cells encapsulated in alginate. (II) Representative macroscopic plan view of the hybrid constructs after 3 and 28 days in culture. (III) Young's modulus. (IV) Biochemical analysis at day 28 for DNA, collagen and sGAG.[49] (Copyright © 2020. The Authors. Published by Elsevier Ltd on behalf of Acta Materialia Inc.)

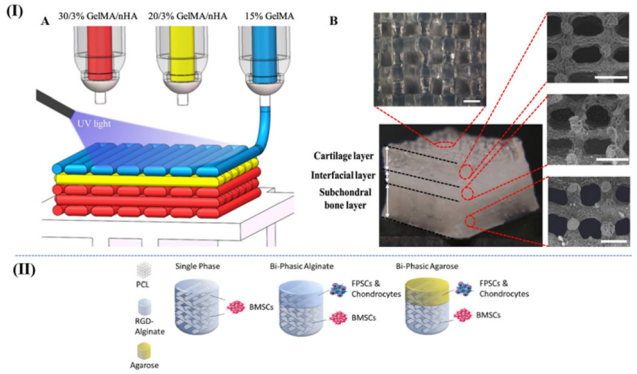


Fig. 8 (I) (A) Schematic of the three-phase layered scaffold printing (30/3% GelMA/nHA for subchondral bone layer, 20/3% GelMA/nHA for interfacial layer, and 15% GelMA/nHA for cartilage layer). (B) Top view and side view of tri-layered scaffold (scale bar is 500 μm)[115] (Copyright © 2019, The Authors. Published by Elsevier Ltd.). (II) Schematic of the multiphase scaffolds in Susan *et al.*'s work[49] (Copyright © 2020. The Authors Published by Elsevier Ltd on behalf of Acta Materialia Inc.).

and reasonably solve the problem of insufficient mechanical properties of natural bio-ink.

In the field of cartilage tissue repair, artificial polymers with strong biocompatibility and degradability, such as PCL and PLA, have emerged as the preferred option for SLS technology. As early as 2011, Shuai *et al.* began using the SLS technology to print blended materials composed of PCL and ceramic particles for osteochondral repair research.[116] Du *et al.* proposed a biomimetic multi-layer cartilage scaffold prepared using polycaprolactone (PCL) and hydroxyapatite (HA)/PCL microspheres. The SLS technology endowed it with a carefully designed structure with gradient composition and low printing material requirements.[62] A cylindrical scaffold with large pores is designed to resemble a cartilage to subchondral bone biomimetic structure, while also ensuring a continuous HA component gradient. Layer separation, a common issue with conventional multi-layer scaffolds, can be resolved by using the SLS technology of printing various microspheres to fabricate continuous transition gradient structures, while guaranteeing mechanical properties (a compression modulus and a compressive strength of 8.7 MPa and 4.6 MPa, respectively). In addition to macroscopically designed macroporous structures with pore sizes ranging from 400 to 500 μm, a large number of interconnected microporous structures with porosity of 60.3% were generated by sintered microsphere fusion, which could better support cell migration and cell attachment *in vitro*. GU *et al.* reported that they used an improved S/O/W emulsion solvent evaporation method to prepare two PCL microspheres with different particle sizes of 50 and 150 μm, designed non-channel-, continuous channel- and non-continuous channel-integrated osteochondral scaffolds.[63] The scaffolds were constructed using the SLS technique, selecting microspheres with s small particle size (PCL50) for the 0.5 mm cartilage region and larger PCL150 for the 2.5 mm subchondral bone region.

PEG is a polyether polymer formed by dehydration and condensation of ethylene glycol. The hydroxyl active group at the end is easy to react with a variety of chemical substances, and has good hydrophilicity and modifiability. Because of its outstanding biocompatibility and stable mechanical properties, it has a great potential in the field of CTE. Fu *et al.* used polyethylene glycol and polycaprolactone to form block copolymers, and the scaffolds significantly improved the recruitment ability of stem cells.[117] Bruna *et al.* attempted to use an interpenetrating polymer network (IPN) hydrogel composed of light-induced cross-linked PEG and cationic physically cross-linked alginate as the main body of CTE scaffold, in an effort to provide a self-healing support bath for subsequent functionalized printing structures.[55] This IPN network hydrogel based on PEG can not only absorb a large amount of water but also retain considerable mechanical properties including rigidity, toughness and viscoelasticity, which provides a potential solution for cartilage tissue repair. All of the studies on CTE scaffolds described above have chosen extrusion-based biological 3D printing (especially DIW) as the way to process the biomaterials reported in this paper. There has been an obvious tendency to combine synthetic materials with natural materials, which have complementary advantages and disadvantages. Of course, it does not imply that these materials can only be employed in a single method to print scaffolds.

Poly (1,3-trimethylcarbonate) (PTMC) is a flexible, biodegradable and amorphous polymer synthesized by ring-opening polymerization of 1,3-trimethylcarbonate. Because PTMC promotes surface erosion through enzymes, it can still maintain mechanical strength and elastomeric properties during degradation,[22,23] but its initial mechanical strength is generally low. In addition, PTMC does not produce acidic byproducts when degraded, which has been recognized as a great advantage in tissue reconstruction.[24,118] However, it is highly hydrophobic and lacks cell recognition sites, which leads to difficulties in cell adhesion.[119] Therefore, it is necessary to improve the mechanical strength of PTMC and its significant affinity for water.

Liu *et al.* prepared PTMC networks by vacuum gamma radiation using trimethylolpropane triacrylate (TMPTA), pentaerythritol triacrylate (PETA) and pentaerythritol tetraacrylate (PET4A) as crosslinking agents to improve mechanical properties and creep resistance.[23] The maximum tensile strength of the PTMC cross-linked network can reach 25.95 ± 2.20 MPa. However, its degradation rate is slow and it still retains more than 90% of its mass after 12 weeks of *in vitro* enzymatic degradation (the degradation performance of scaffolds is also recorded in Table 2, which also includes the degradation performance of scaffolds in other studies). Thomas *et al.* synthesized gAR-*graft*-poly(trimethylene carbonates) (gel-*g*-PTMC*n*) and successfully manufactured 3D porous objects using stereolithography. To demonstrate the great potential of this bioresin in tissue engineering.[61] Compared with PTMC or gelatin, tensile Young's modulus of gel-*g*-PTMCN was significantly improved (gel: 0.74 ± 0.13 MPa, PTMC: 1.29 ± 0.17 MPa, and gel-*g*-PTMC: 4.62 ± 0.84 MPa). In order to ensure that the resin has the right viscosity (1–10 Pa s), they diluted it with 40% dimethyl sulfoxide (DMSO) solution, resulting in a polyporous

Table 2 Scaffold degradation behaviour of various biomaterials

| Processed materials | Test period | Index of sample testing | Degradation property | Ref. |
|---|---|---|---|---|
| Alg/NC/Chs/DS | 10 days | Scaffold area retention rate | NC-Alg-CS: 73 ± 3.40%, NC-Alg-DS: 79.85 ± 0.05%, and NC-Alg: 78.62 ± 7.21% | 51 |
| Alg/nHA/CS | 28 days | Degradative weight loss ratio | Ratio maximum: ~30% | 52 |
| PLGA | 12 weeks | Degradative weight loss ratio | 75.70% | 53 |
| Alg/PEG | 25 days | Reduction of compressive modulus after degradation | Maximum reduction: 78 times (1.05 ± 0.17/4.43 ± 0.21 MPa) | 55 |
| PGD/APGD | 28 days | Degradative mass remaining ratio | ~80% | 56 |
| EVO/PCO | 3 months | Observing the tissue at the placement of the elastomer | Complete degradation | 120 |
| PLA/ABS | 21 days | Reduction of compressive modulus after degradation | ABS: ~197 kPa and ~193 kPa (0 d and 20 d), PLA: ~520 kPa and ~560 kPa (0 d and 20 d), and no significant difference | 64 |
| Alg/ALG-SUL/dECM/PCL | 28 days | Degradative weight loss ratio | ~17% | 65 |
| GelMA/PTMC | 8 hours | Degradative mass remaining ratio | 0% | 61 |
| PTMC/TMPTA/P,ETA/PET4A | 12 weeks | Degradative weight loss ratio | <10% | 23 |
| PU/HA | 28 days | Degradative mass remaining ratio | ~60% | 57 |
| PU | 28 days | Degradative mass remaining ratio | ~60% (PU: 61% and PU/SDF-1/MS_Y: 58.3%) | 58 |
| PCL/PLA/nHA | 30 days | Rate of mass loss from enzymatic degradation | 0.35 ± 0.05% (blank) and 0.33 ± 0.09% (nHA) | 67 |

cube with a layer thickness of about 100 μm and high shape accuracy.

Polyurethane (PU) is one of the most popular synthetic biomedical polymers due to its excellent biocompatibility, tunable chemical structure and good mechanical properties.[121] As a common 3D printing material, PU has good flexibility and the data of 3D printed PU stent after cyclic loading show high elasticity,[122] which can imitate the mechanical properties of soft tissues. However, PU is usually dissolved in toxic organic solvents,[123] which makes the final product difficult to print because of the residual solvent.[124] Biodegradable PU can be prepared using water-based processes. Hung *et al.* and Wen *et al.* reported waterborne polyurethane, using a direct ink writing method to prepare scaffolds suitable for cartilage tissue engineering. In Hung *et al.*'s study,[57] in order to facilitate printing, PU and HA aqueous solution were mixed (mass ratio 76 : 24) and the compression modulus of the printed PU-HA scaffold was 0.33 ± 0.02 MPa, and it showed excellent dimensional recovery ability under 10% cyclic compression strain. In biological experiments, MSCs seeded on scaffolds self-assembled into MSC aggregates and effectively generated cartilages. The compression modulus of the scaffold prepared by Wen *et al.* was about 0.94 ± 0.01 MPa. Despite ensuring mechanical properties, its degradation ability was also excellent. After degradation *in vitro* for 28 days, the retained mass was about 60% of the initial mass.[58]

### 3.3. Biologically inspired copolymer elastomer

The first two parts of this chapter described the application of synthetic materials (engineering plastics) and natural materials (hydrogels). However, because mechanical properties and biological factors need to be reconciled, they are not usually used in tissue engineering stents alone. For the mixed-use of the two types of materials, in addition to their mechanical mixing together, there is also a common polymerization method to form a polymer chain.

Biologically inspired elastomers are an important part of cartilage tissue engineering. A considerable number of studies have been conducted using naturally occurring monomers copolymerized with the monomers of synthetic polymers and the polymer materials they form are made into elastomers. Polydiol citrate (POC),[125] polyglycerol sebacate (PGS),[126] polyglycerol dodecane dicarboxylate (PGD),[56] epoxy vegetable oil,[127] and other materials are expected to play a role in cartilage tissue engineering.

Polydiol citrate (POC) is an elastic polyester that can be obtained from the polymerization of citric acid and 1,8-octandiol. Its promising properties, such as high elasticity, hydrophilicity, linear degradation curve, and biocompatibility, make it ideal for potential clinical applications in soft tissue engineering.[128–130] The degradation rate and mechanical properties of POC are affected by many factors (such as curing time, temperature, and initial monomer number), which can be adjusted to simulate the elastic properties of soft tissues.[131] However, in some reports, POC's mechanical properties (Young's modulus and tensile strength) are weak and their degradation products may also reduce local pH, leading to inflammatory responses.[132] The above two problems also limit the application of POC in tissue engineering.

Ehsan *et al.* used a solid solution pouring method to blend different proportions of POC with chitosan (CS) to prepare films of different components to manipulate their physicochemical properties.[125] Firstly, the weak mechanical properties were solved by the addition of CS: with the increase of the CS content, the thickness of the blend film gradually became thinner (from 386 μm to 106 μm), but the tensile strength increased continuously (0.29 MPa to 33.61 MPa). Secondly, the problem of degradation causing pH reduction is improved: after 7 days, the pH changes of phosphate buffered saline (PBS, pH = 7.4, resistant to a certain degree of pH changes) gradually stabilized and the membranes containing more CS showed higher pH stability. The pH of pure POC dropped

 

sharply to 5.85. In Sara *et al.*'s study, a mesoporous bioactive glass (MBG) was selected to improve the physicochemical properties and degradation behavior of POC.[130] The therapeutic trace element Ag improves the composition of MBG and its excellent antimicrobial potential helps the tissues surrounding the implant in overcoming microbial infection. Ag-containing mesoporous bioactive glass (AgMBG) was introduced in the form of particles to prepare a composite porous scaffold based on POC. A larger AgMBG particle load can improve the mechanical properties of the scaffold. Compared with the compressive elastic modulus obtained by compression test, the mechanical properties of 20 wt%AgMBG/POC scaffolds increased to about 5 times that of pure POC (6.93 KPa *vs.* 33.95 KPa), which was considered to be due to the electrostatic interaction between AgMBG particles and POC, which improved the cross-linking density of scaffolds. The composite porous scaffold was immersed in Tris–HCl buffer for 28 days to record the pH value of the solution. After loading AgMBG particles, the pH value of the solution did not decrease, which compensated for the disadvantage of the POC scaffold degrading the local pH value and causing inflammation.

Polyglycerol sebacate (PGS) is synthesized based on the polycondensation reaction of glycerol and sebacic acid and it is a biologically absorbable material because its polymeric monomers are natural ingredients (glycerol is a basic component of lipids, sebacic acid is a natural metabolic intermediate of the oxidation of medium-long chain fatty acids $\omega$). The adjustable degree of esterification determines the variable mechanical properties and degradation behavior of the polymer.[133] PGS is non-immunogenic and has been shown to be non-cytotoxic *in vitro* and cause only minimal inflammatory responses. These excellent properties have earned PGS its status as a soft tissue regeneration scaffold material.[134]

Dan Lin *et al.* combined pegylated polyglycerol sebacate (PEGS) with MBG to construct a PEGS/MBG double-layer scaffold and evaluated it in a cartilage defect model.[126] The copolymerization of PGS and PEG improves the hydrophilicity, and Young's modulus of PEGS with a low crosslinking degree (shortening the crosslinking time to 12 h) is $\sim$0.6 MPa, and provides the viscoelasticity, mimics the mechanical microenvironment of cartilage matrix, and can significantly stimulate cartilage differentiation and enhance the secretion of cartilage matrix. At the same time, MBG, as one of the foci of bone repair scaffolds, has a great advantage in subchondral bone reconstruction due to its positive bone inductivity and biodegradability. The MBG scaffolds prepared in this study showed a high compressive strength ($\sim$5 MPa) and irreversible brittle fracture under compression, which are similar to the mechanical properties of femoral trabeculae. PEGS/MBG double-layer scaffolds provide guidance for differentiating of cartilage and osteogenesis, respectively, and can achieve synchronous repair of cartilage and subchondral bone. In the study, PEGS/MBG double-layer scaffolds were inserted into the bone and cartilage defect with a diameter of 6 mm at the femoral patellar groove joint of a rabbit. 12 weeks later, micro-CT observation showed that compared with the blank group and the single-layer PEGS scaffold group, only the double-layer scaffolds formed completely closed subchondral bone and the trabecular thickness was the highest (426.83 μm). The percentage of bone volume was the highest (BV/TV = 87.78%), showing remarkable cartilage and subchondral bone regeneration.

Polyglycerol dodecane dicarboxylate (PGD) is a biodegradable thermosetting polyester, which is synthesized by polycondensation of non-toxic monomer glycerol and dodecane dicarboxylic acid to produce biocompatible by-products. It has shape memory properties and achieves nonlinear elasticity of soft tissues at transition temperatures close to body temperature, with tangential elastic modulus ranging from 0.5 to 5 MPa and elastic deformation of 70–80%.[135–137] The transition temperature and mechanical properties of PGD can be adjusted by its synthetic parameters (curing time and temperature) and can be used to design degradable implants. This biodegradable polyester, which is affected by enzymes as it degrades *in vivo*, can lose 50% of its own mass in four months (it takes about 16 months for the same weight to be lost *in vitro*).[135] However, PGD is hampered by harsh curing conditions (high temperature and vacuum), which limits the strategy of cartilage tissue engineering to maintain the mechanical properties of scaffolds, while creating connected porous structures.

Rayan *et al.* explored the use of acrylic acid chemistry to produce photocurable PGD, which can solve some clinical problems that require *in vivo* curing without thermal curing conditions.[56] The crosslinking density of this photocurable PGD (APGD) is affected by the acrylic acid content (Acr%) and increases with the increase of its mass fraction, so APGD samples with higher Acr% should have greater Young's modulus. However, in the tensile test of APGD dog bone samples, there is no significant difference between Young's modulus and fracture strain, and it is believed that the addition of Acr reduces the shape memory transition temperature, and the elastic rubberization degree is improved due to the shape memory effect at the preset 37 degrees Celsius, which cancels the original increase in stiffness. Even so, APGD still maintains an elastic modulus of $\sim$5 MPa. Thin films made using APGD showed good cell viability, and NIH3T3 cells proliferated significantly 14 days after inoculation, demonstrating the applicability of this material in soft tissue engineering. They also attempted to use the DIW method to fabricate scaffold structures with line widths of 250, 300, and 400 μm, conducting initial validation of 3D printing applications.

Vegetable oils are a class of rich renewable resources, such as soybean oil, palm oil, flaxseed oil, castor oil, *etc.*, and they are mainly composed of glycerol and esterified unsaturated fatty acid, because they are unsaturated theoretically they can be directly used as a polymeric monomer. Unfortunately, photoinduced radical polymerization of these oils either does not occur or is very slow at the application level. Therefore, vegetable oils are often converted into epoxides.[138] Of course, the more common epoxidized vegetable oils generally use active groups such as double bonds, hydroxyl groups, and ester groups in the structure of vegetable oils, which are converted into highly active photocurable monomers or prepolymers through chemical modifications. Some typical modification

methods include acrylylation, epoxidation of unsaturated double bonds, ethylene acylation, amidation, *etc*.[139] Elastomers prepared from epoxy vegetable oils have good mechanical properties, biodegradability, and low toxicity, and because they can be polymerized by ultraviolet irradiation, SLA, DLP and other printing methods are highly adapted to them and scaffolds with high structural accuracy can be constructed, which have great potential in soft tissue engineering.[138,140]

To increase the reactivity of vegetable oils and pay attention to their toxicity, Diego *et al.* prepared the epoxide of vegetable oil (hydrogen peroxide and formic acid are epoxidized) and multi-component photoinitiated catalysts (phenylbis (2,4,6-trimethylbenzoyl) phosphine oxide (BAPO), curcumin, *etc.*) were synthesized to promote UV polymerization. In subsequent photocurable printing tests, they also added a light absorbent (0.1 mg $mL^{-1}$) and a cationic active diluent (tri(ethylene glycol) divinyl ether, 20%) to the epoxy vegetable oil.[138] The addition of these components is necessary: the former facilitates deep polymerization; the latter reduces the viscosity of the epoxy plant oil-based resin, facilitates the formation of a liquid layer in the printing material, and reduces the shear stress during the printing process. Anda *et al.* used an SLA printer to produce cubes printed with soybean oil epoxidized acrylic (AESO). AESO eliminates toxicity concerns of petroleum acrylates, provides high printing accuracy and resolution (25 μm) and the introduction of acrylic groups solves the shortcomings of the high viscosity of epoxidized vegetable oil.[127] At the same time, thermal stability also affects the processability and application range of the polymer and researchers also tried to introduce two reactive monomers, 1,6-hexadiol diacrylate (HDDA) and trimethylipropane triacrylate (TMPTA) to adjust the 3D printing conditions and improve the thermal properties of the photocurable polymer. With the addition of the copolymer, the thermal stability of AESO photocurable resin is greatly improved, the glass transition temperature is increased by more than 10 °C, and the maximum thermal degradation temperature is increased by 28 °C.

Liu *et al.* reported the preparation of biocompatible and biodegradable phosphate ester cross-linked vegetable oil (PVO) elastomers, which are prepared without the addition of any solvents and initiators. They are prepared by a simple cross-linking reaction between phosphorylated castor oil (PCO) and epoxidized vegetable oil (EVO), epoxidized soybean oil (ESO) and epoxidized linseed oil (ELO).[120] They evaluated the mechanical properties of PVO. In the tensile test of dog bone samples, Young's modulus of PVO showed a trend of first increasing and then decreasing with the increase of the epoxide ratio and the highest modulus was 3.05 MPa. In the compression test, the PVO elastomer also has a good compressive strength (0.65 MPa) and the maximum deformation is more than 50%. PVO elastomers show excellent elasticity in cyclic compression tests, that is, after 1000 compressions, the stress–strain curve is almost repeatable and quickly returns to its original shape. In addition, PVO had low cytotoxicity, and the cell relative viability was greater than 0.85 after 3 days of L929 cell line culture. At the same time, in rats, PVO is completely degraded and absorbed within 3 months and there is only a very slight inflammatory reaction during the whole process. These characteristics show the application prospects of the PVO elastomer in soft tissue engineering.

# 4. The functional design of CTE scaffolds

## 4.1. Release of bioactive factors

Several bioactive factors, most of which are synergistic or complementary: they comprehensively govern the process of tissue response, integration and healing; they are also required for the differentiation of stem cells into mature chondrocytes.[6,141] In the existing TE research, it is generally adopted to directly add exogenous bioactive factors or implant the scaffold loaded with factors to enhance the proliferation and differentiation ability of stem cells, hence promoting the repair and reconstruction of the injured site. Growth factors, transitive genes, and small molecule medicines are frequently considered to be bioactive factors in biochemistry.[141] The classification of biochemical factors and their effect on the tissue during cartilage treatment are recorded in Table 1 below.

After the occurrence of articular cartilage injury, the self-healing ability is poor. By adding exogenous bioactive factors in the scaffold, they can induce MSCs to differentiate into chondrocytes, promote the continuous proliferation of cells, and obviously contribute to the repair of cartilage injury (although the types of factors are different, they are synergistic or complementary in the physiological activities of cartilage reconstruction. This also provides favorable conditions for the combination of multiple growth factors).

## 4.2. Seed cells provide renewable resources

In the TE scaffold strategy, osteoblast is an important problem to be reckoned with, cartilage defects are a very complex and diverse issue with different locations, types, and degrees of severity.[142] The success of the bracket design strategy depends on closely examining the cell proliferation differentiation situation and even the seed cells determine the quality[143] of the tissue regeneration. Due to the limited regenerative capacity of human tissue, TE technology uses the method of seeding cells on biodegradable scaffolds to create cell-scaffold constructs to complete tissue self-healing and regeneration.[144] The cells involved in this process are called seed cells. In clinical practice, when selecting and obtaining seed cells, doctors first consider the adequacy of the cell source, then speculate the stability of reconstructed cartilage, and finally judge the severity of donor injury.[144,145] Of course, the clinical selection is conditional on cells of this type having no or only weak immune rejection and possessing the ability to produce tissue-specific ECM proteins.[141,144,145]

Chondrocytes, embryonic stem cells, mesenchymal stem cells, and induced pluripotent stem cells are among the seed cells commonly employed by CTE researchers. They come from autologous or allogeneic sources. According to the

 

Table 3 Types and efficacy of bioactive factors

| Types of bioactive factors | Description | Efficacy on osteochondral units | Ref. |
|---|---|---|---|
| Growth factor | TGF-β (subtypes 1/2/3) | Promoting the differentiation of stem cells into chondrocytes and maintaining their homeostasis; inhibition of cartilage hypertrophy and degeneration; to promote cartilage extracellular matrix synthesis and hyaline cartilage formation | 110,114,146,147 |
| | FGF (subtypes 2/18) | Stimulating the up-regulation of endogenous TGF-β, BMP, VEGF and SOX9 to help in repairing cartilage injury; it is beneficial to stem cell differentiation and chondrocyte enrichment | 148,149 |
| | IGF-1 | Promoting cell proliferation and synthesis of aggrecan type II collagen; activation of PI3K-AKt pathway helps MSC migration in achieving cartilage repair | 150,151 |
| Transitive genes | BMP (subtype 2/4) | A genetic protein that induces the differentiation of stem cells and helps in chondrogenesis; it promotes anabolism and catabolism, increases ECM production, inhibits cartilage hypertrophy and maintains cartilage phenotype | 6,152,153 |
| | SOX9 | It influences the expression of genes important for chondrogenesis and plays a key role in chondrocyte differentiation | 154,155 |
| | Runx-2 | Binding to the promoter of osteocalcin to regulate chondrogenic differentiation | 156 |
| Small molecule drugs | Dexamethasone (DEX) | It is often used as a supplement to TGF or BMP to further promote cell proliferation and maximize chondrogenic induction to achieve the best chondrogenic or osteogenic effect | 157 |
| | Y27632 | Inhibiting apoptosis of MSCs; promoting the differentiation of cartilage hormones | 158 |
| | Ascorbic acid | It promotes chondrocyte proliferation and chondrocyte protein secretion | 159 |
| | Berberine chloride | Stimulating chondrocyte proliferation; enhancing aggrecan and Col II expression | 160,161 |
| | Lysophosphatidic acid | Promoting chondrocyte proliferation; enhancing cell survival | 161,162 |

differentiation state of cells, they can also be divided into mature adult cells and stem cells with differentiation potential.

### 4.3. Other functions

Seed cells and bioactive factors are the two most concerning issues for researchers in the field and they are also the most easily considered factors for the design strategy of TE scaffolds. However, for some special application scenarios, more ideas about functionalization have been developed and progressively more people are becoming aware of it (Table 3).

Facing a huge challenge of tissue reconstruction after chondrosarcoma surgery, Zhu *et al.* developed a multifunctional hydrogel that can be directly written and printed with the assistance of photocrosslinking for this application scenario.[163] In their research, repair of defective tissue, tumor recurrence, and bacterial infection are three issues that may arise in this application scenario. To overcome these challenges, methacrylic anhydride-modified silk protein (SerMA) solution was prepared and mixed with proanthocyanidin-loaded zeolite imidazolate-skeleton 8(ZIF-8) nanoparticles modified by polydopamine (PDA) to obtain a PC@ZIF-8@PDA/SerMA hydrogel. The PC@ZIF-8@PDA nanoparticles are the major part for achieving the multifunctional function of scaffolds: PC has good antibacterial and anti-inflammatory effects; PDA, as a photothermal agent with high photothermal conversion efficiency,[164] makes tumor thermotherapy possible. ZIF-8 is a pH-responsive metal–organic framework (MOF) that has been frequently reported as a drug delivery vehicle.[163,165–167] SerMA solution loaded with nanoparticles can promote the repair of damaged cartilage tissue. The complex material design endows this hydrogel with the ability to promote tissue repair, spatiotemporally controlled release of drugs, antibacterial and anti-inflammatory properties, and photothermal killing ability of tumor cells, opening up new avenues for future scaffold functionalization research.

## 5. The architectural design of CTE scaffolds

For a long time, it has been the goal of researchers to construct cartilage scaffolds with ideal performance successfully. In addition to mechanical proximity to natural cartilage, cartilaginous engineered scaffolds require suitable macroscopic and microporosity for cellular attachment and transport of nutrients/wastes.[168] The next-generation CTE scaffolds also require biodegradability based on biocompatibility, allowing them to be automatically eliminated from the body after tissue restoration without harming other organs and tissues.[168] Except for biomaterials that can affect the repair function of scaffolds, the design of the structure is another area of intense focus. Porous structures with suitable pores and ideal mechanical properties can accurately mimic the complexity of natural cartilage units, which can also encourage the generation of new tissues.[169]

### 5.1. Gradient structure design

The gradient architecture strategy has advanced quickly in recent years, moving from straightforward single-phase scaffolds to more complex biphasic and multiphase scaffolds with continuous gradients in an ongoing effort, which mimic the spatial structure and mechanical characteristics of various cartilage layers.

Single-phase scaffolds represent the earliest design standard for osteochondral repair technology in structural problems. A single biomaterial is arranged in the defect area with a single

structure, which initially mimics the structure of cartilage tissue, in an attempt to achieve ideal structural strength and porosity.[170,171] Material homogeneity shows that the scaffold as a whole has the same material in the same proportion of components rather than implying that only one material is employed (as is the inclusion of a supplementary gel phase in the void of the entire scaffold[172]). The PLA stent prepared in Derek *et al.*'s study mentioned above[64] is the most typical single-phase stent. Many studies have shown that monophasic scaffolds can support the attachment and proliferation of osteoblasts to a certain extent, but their ability is very limited, which is difficult to support the partition regeneration of cartilage and subchondral bone at the same time.

Stratified multiphase scaffolds are the mainstream of current research, including biphasic, triphasic, and continuous gradient phases.[173] They are regarded as the best osteochondral scaffolds because of their improved composition, structure, and mechanical qualities. The different structural layers of the osteochondral unit, mainly cartilage, and subchondral bone, have been well accounted for, even when calcified layers of cartilage tissue are involved, further toward the hierarchy of native cartilage.

Compared with monophasic scaffolds, layered multiphase scaffolds have greater advantages: (1) appropriate growth factors can be added in different layers to simulate cartilage and bone tissues with different pre-cultured seed cells;[174] (2) different types of chemical, mechanical, and biological stimuli conducive to cell proliferation/differentiation can be provided; and (3) appropriate microenvironments can be constructed more precisely to guide cell/cell and cell/matrix communication.[175] Thunsiri *et al.* proposed a bilayer scaffold prepared from biomaterials.[67] The cartilage (AC) layer was composed of polylactic acid (PLA) and polycaprolactone (PCL) hybrid fibers, which were 3D printed and freeze-dried with chitosan (CS)/filamentous fibers (SF), and the subchondral bone layer was simulated by PLA, PCL, and 15% (wt%) nHA. The addition of nHA significantly increased the compressive stress of the subchondral bone layer compared with the AC layer; the cell viability of PCL/PLA/15nHA was also higher (177.18 $\pm$ 2.87% and 277.21 $\pm$ 16.93%) than that of the control group (PCL/PLA), a similar situation (158.62 $\pm$ 16.61% and 308.28 $\pm$ 7.88%) occurred after CS/SF treatment compared with before treatment in the AC layer.

The three-phase layered scaffold introduces a calcified cartilage simulation layer based on the second phase. The newly added layer helps in supporting a load of articular cartilage, whilst also serving as a physical barrier, inhibiting vascular invasion, preventing ossification of full-thickness cartilage, and comprehensively regulating the tissue integration ability of the contact section between the implanted scaffold and host tissue.[176] Li *et al.* designed a biomimetic three-layer fiber-reinforced hydrogel scaffold[177] and fabricated a PLGA/β-TCP composite into a three-phase CTE scaffold using a low-temperature assisted DIW. It was also proposed in their work to attempt inoculating MSCs *in vitro*, and they attached the three layers using "lytic adhesion technology" to create stable three-layer biomimetic scaffolds.[177] Biological experiments showed that the number of cells in the scaffolds increased synchronously with the increase of experimental time and a stable plateau of cell proliferation began to appear from 7 to 11 days. When observed by SEM, there were differences in the cell morphology between the cartilage layer and the bone layer of the scaffold (in human tissues, the cell morphologies of different layers of cartilage are also different). These results partly confirm the role of the introduced calcified layer as an osteochondral interface: the calcified layer can successfully isolate the bone and cartilage microenvironment and minimize their interaction. Whereas they did not study the effect of calcified layers, such as reducing vascular invasion into the cartilage layer of the scaffold, and they also mentioned in the article that they will continue to improve the research. However, the gradient between each level of the three-phase layered scaffold is discrete, which cannot mimic the smooth transition between tissues and does not have a clear interface.[178]

Continuous gradient transition has greater adaptability to most natural conditions, which can improve load transfer and avoid interfaces with potentially unstable mechanical properties. Sun *et al.*[179] concluded that region-dependent chondrogenic differentiation and ECM deposition can be induced by biomimetic structures that replicate gradient anisotropic structures and signaling techniques in various layers. Continuous gradient scaffolds do not exhibit independent layer structures, but are manufactured as a single matrix with gradient properties,[180–182] which avoids stratification during loading. This structure promotes chondrogenic/osteogenic differentiation and ECM deposition of BMSC (or other seed cells). Continuous gradient scaffolds are developed by buoyancy, magnetic attraction, and electrical attraction techniques;[183–185] they have a gradual transition between different areas of the structure. These scaffolds are preferable to monophase, biphasic, and general multiphase scaffolds in the restoration of osteochondral lesions because they can more accurately mimic the natural features of the joint. Similarly, the preparation of continuous gradient scaffolds is also considerably more challenging and relevant studies still need to be carried out.

### 5.2. Balance between porosity and mechanical properties

Designing a TE scaffold for chondro-bone interfaces requires accurate representation of load and stress distributions, spatiotemporal controlled release of biochemical factors, and graded porous structures. Interconnected open pores are more conducive to cell migration and nutrient flow.[186–189] In addition to requiring scaffolds to use biomaterials that match the mechanical properties of native tissues, the osteochondral tissue exhibits an ordered structure with varying degrees of mineralization and pore size that a successful scaffold must precisely mimic.[187,190,191] In short, scaffolds need to strike a balance between suitable pores and the mechanical properties of native cartilage tissue, which means that they should be met simultaneously. Traditional TE does not have a solution to this intractable problem. Some manufacturing technologies (such as foaming, electrospinning, and freeze-drying) are stochastic in the preparation of high-performance porous structures and it is difficult to control the distribution of diverse composite material components in 3D

 

space.[192–195] The development of 3D bioprinting has given a new approach to the academic community.

Sean M. Battner *et al.* varied the vertical gradients of scaffold porosity and the ceramic content to mimic the changes in composition and pore morphology in native osteochondral units in developing a PCL-HA scaffold.[196] Meanwhile, they evaluated the printing reproducibility and scaffold structure for inclusion in the study. The printed structures were then subjected to uniaxial mechanical compression to assess the effect of scaffold porosity and ceramic content on their mechanical properties (compressive modulus and yield stress). It was found that the compression modulus and yield stress of the small hole (0.2 mm) scaffolds were significantly higher than those of all other groups after grouping, while there was no significant difference in compression modulus and yield stress between the medium hole (0.5 mm) and large hole (0.9 mm) scaffolds. In the same aperture group (0.2 mm, 0.5 mm, and 0.9 mm), the compressive modulus and yield stress are independent of the ceramic content, indicating that the incorporation of ceramic gradient does not significantly affect the structure's mechanical properties. The uniaxial compression test shows that the porosity, compressive modulus, and yield stress are inversely proportional. The porosity gradient scaffolds exhibit similar compression properties to the scaffolds with the highest porosity fraction, indicating that these properties are more influenced by the weakest part of the gradient.

## 6. Challenges and future perspectives

Cartilage injury is a serious clinical challenge because of the high prevalence of injury, the presence of only a small number of cells in cartilage, and the poor intrinsic healing ability.[197] Considering the stratified structure of osteochondral tissue, injured tissue reconstruction remains a major challenge. For example, articular cartilage and subchondral bone are unified functional units; the conflict between the ischemic and nonneuronal character of hyaline cartilage and the vascular richness of subchondral bone needs to be resolved. The complex structure and biomechanical properties of osteochondral tissue bring great challenges for the construction of TE substitutes with high fidelity to native tissues. In addition to scaffold manufacturing, cell differentiation and cell patterning are also important factors in the process of regeneration. Appropriate manual intervention for cell differentiation at different levels of regions should be considered.

As a revolutionary manufacturing process, 3D printing offers many opportunities for advancement in the field of CTE. At present, the main problem in terms of technology is how to improve printing resolution, printing speed, and processing costs. Without a doubt, the expansion of biomaterials, the selection of seed cells, and the adaptation of bioactive substances are also crucial.

## Conflicts of interest

The authors have no conflicts of interest to declare.

## Acknowledgements

This research was supported by the Zhejiang Provincial Natural Science Foundation of China under Grant No. LZ22E030003, the Ningbo Natural Science Foundation of China (2022J231, 2023J050), the National Key Research and Development Project of China (2021YFB3701500), and the National Natural Science Foundation of China (52273241).

## Notes and references

1 A. Weizel, T. Distler, D. Schneidereit, O. Friedrich, L. Brauer, F. Paulsen, R. Detsch, A. R. Boccaccini, S. Budday and H. Seitz, *Acta Biomater.*, 2020, **118**, 113–128.
2 A. A. Elhadad, A. Alcudia, B. Begines, E. M. Perez-Soriano and Y. Torres, *Appl. Mater. Today*, 2022, **29**, 21.
3 R. F. Loeser, S. R. Goldring, C. R. Scanzello and M. B. Goldring, *Arthritis Rheum.*, 2012, **64**, 1697–1707.
4 G. C. Gurtner, S. Werner, Y. Barrandon and M. T. Longaker, *Nature*, 2008, **453**, 314–321.
5 R. F. Loeser, S. R. Goldring, C. R. Scanzello and M. B. Goldring, *Arthritis Rheum.*, 2012, **64**, 1697–1707.
6 Y. F. Ao, *Articular cartilage repair and restoration*, Peking University Medical Press, Beijing, 2020.
7 F. Berenbaum, *Osteoarthr. Cartil*, 2013, **21**, 16–21.
8 L. A. Mandl, *Osteoarthr. Cartil.*, 2019, **27**, 359–364.
9 A. Trengove, C. Di Bella and A. J. O'Connor, *Tissue Eng., Part B*, 2022, **28**, 114–128.
10 R. Teshima, K. Nawata, H. Hagino, Y. Morio, M. Inoue and Y. Irizawa, *Acta Orthop. Scand.*, 1999, **70**, 381–386.
11 M. Mostakhdemin, A. Nand and M. Ramezani, *Polymers*, 2021, **13**, 13122000.
12 A. A. Elhadad, A. Alcudia, B. Begines, E. M. Perez-Soriano and Y. Torres, *Appl. Mater. Today*, 2022, **29**, 101603.
13 A. J. Sophia Fox, A. Bedi and S. A. Rodeo, *Sports Health*, 2009, **1**, 461–468.
14 Z. H. Wang, H. X. Le, Y. B. Wang, H. Liu, Z. H. Li, X. Y. Yang, C. Y. Wang, J. X. Ding and X. S. Chen, *Bioact. Mater.*, 2022, **11**, 317–338.
15 R. Chen, S. Chen, X. M. Chen and X. Long, *Arch. Oral Biol.*, 2011, **56**, 1390–1397.
16 Y. F. Ao, Z. Li, C. C. Zhang and X. J. Duan, *Orthop. J. China*, 2019, **27**(08), 722–725.
17 K. Li, C. Q. Zhang, L. L. Qiu, L. L. Gao and X. Z. Zhang, *Tissue Eng., Part B*, 2017, **23**, 399–411.
18 W. Z. Zhu, Y. J. Chuah and D. A. Wang, *Acta Biomater.*, 2018, **74**, 1–16.
19 Y. Zhao, H. Liang, S. Q. Zhang, S. W. Qu, Y. Jiang and M. F. Chen, *Polymers*, 2020, 12.
20 Y. Ramot, M. Haim-Zada, A. J. Domb and A. Nyska, *Adv. Drug Delivery Rev.*, 2016, **107**, 153–162.
21 N. J. Castro, C. M. O'Brien and L. G. Zhang, *AIChE J.*, 2014, **60**, 432–442.
22 Z. Zhang, R. Kuijer, S. K. Bulstra, D. W. Grijpma and J. Feijen, *Biomaterials*, 2006, **27**, 1741–1748.

23 X. L. Liu, S. Liu, K. Q. Li, S. M. Feng, Y. K. Fan, L. J. Peng, X. Wang, D. L. Chen, C. D. Xiong, W. Bai and L. F. Zhang, *Polym. Degrad. Stab.*, 2021, **193**, 109718.
24 J. Wang, Y. H. He, M. F. Maitz, B. Collins, K. Q. Xiong, L. S. Guo, Y. H. Yun, G. J. Wan and N. Huang, *Acta Biomater.*, 2013, **9**, 8678–8689.
25 D. J. Huey, J. C. Hu and K. A. Athanasiou, *Science*, 2012, **338**, 917–921.
26 N. Marom, W. Bugbee and R. J. Williams, *Oper. Tech. Sports Med.*, 2020, **28**, 7.
27 L. Gao, L. K. H. Goebel, P. Orth, M. Cucchiarini and H. Madry, *Dis. Models Mech.*, 2018, **11**, dmm034280.
28 S. Oussedik, K. Tsitskaris and D. Parker, *Arthroscopy J. Arthroscopic Relat. Surg.*, 2015, **31**, 732–744.
29 D. L. Richter, J. A. Tanksley and M. D. Miller, *Sports Med. Arthroscopy Rev.*, 2016, **24**, 74–78.
30 J. W. Belk and E. McCarty, *Arthroscopy J. Arthroscopic Relat. Surg.*, 2020, **36**, 304–306.
31 M. Brittberg, L. Peterson, E. Sjogren-Jansson, T. Tallheden and A. Lindahl, *J. Bone Jt. Surg., Am. Vol.*, 2003, **85A**, 109–115.
32 D. Goyal, A. Goyal, S. Keyhani, E. H. Lee and J. H. P. Hui, *Arthroscopy J. Arthroscopic Relat. Surg.*, 2013, **29**, 1872–1878.
33 S. Z. Nawaz, G. Bentley, T. W. R. Briggs, R. W. J. Carrington, J. A. Skinner, K. R. Gallagher and B. S. Dhinsa, *J. Bone Jt. Surg., Am. Vol.*, 2014, **96A**, 824–830.
34 M. Falah, G. Nierenberg, M. Soudry, M. Hayden and G. Volpin, *Int. Orthop.*, 2010, **34**, 621–630.
35 S. Y. Shin, H. F. Rios, W. V. Giannobile and T.-J. Oh, in *Stem Cell Biology and Tissue Engineering in Dental Sciences*, ed. A. Vishwakarma, P. Sharpe, S. Shi and M. Ramalingam, Academic Press, Boston, 2015, pp. 459–469.
36 E. B. Hunziker, K. Lippuner, M. J. B. Keel and N. Shintani, *Osteoarthr. Cartil.*, 2015, **23**, 334–350.
37 K. M. Park, Y. M. Shin, K. Kim and H. Shin, *Tissue Eng., Part B*, 2018, **24**, 327–344.
38 G. Mazza, W. Al-Akkad, K. Rombouts and M. Pinzani, *Hepatol. Commun.*, 2018, **2**, 131–141.
39 S. P. Tarassoli, Z. M. Jessop, A. Al-Sabah, N. Gao, S. Whitaker, S. Doak and I. S. Whitaker, *Br. J. Plast. Surg.*, 2018, **71**, 615–623.
40 S. V. Murphy and A. Atala, *BioEssays*, 2013, **35**, 163–172.
41 J. N. Fu, X. Wang, M. Yang, Y. R. Chen, J. Y. Zhang, R. H. Deng, Z. N. Zhang, J. K. Yu and F. Z. Yuan, *Front. Bioeng. Biotechnol.*, 2022, **9**, 812383.
42 D. Ozdil and H. M. Aydin, *J. Chem. Technol. Biotechnol.*, 2014, **89**, 1793–1810.
43 K. F. Leong, C. M. Cheah and C. K. Chua, *Biomaterials*, 2003, **24**, 2363–2378.
44 C. K. Chua, W. Y. Yeong and K. F. Leong, Rapid prototyping in tissue engineering: A state-of-the-art report, Leiria, Portugal, 2005.
45 J.-p Seo, T. Tanabe, N. Tsuzuki, S. Haneda, K. Yamada, H. Furuoka, Y. Tabata and N. Sasaki, *Res. Vet. Sci.*, 2013, **95**, 1210–1216.
46 C. Erisken, D. M. Kalyon, H. J. Wang, C. Ornek-Ballanco and J. H. Xu, *Tissue Eng., Part A*, 2011, **17**, 1239–1252.
47 D. Antoni, H. Burckel, E. Josset and G. Noel, *Int. J. Mol. Sci.*, 2015, **16**, 5517–5527.
48 G. L. Ying, N. Jiang, C. Parra-Cantu, G. S. Tang, J. Y. Zhang, H. J. Wang, S. X. Chen, N. P. Huang, J. W. Xie and Y. S. Zhang, *Adv. Funct. Mater.*, 2020, **30**, 2003740.
49 S. Critchley, E. J. Sheehy, G. Cunniffe, P. Diaz-Payno, S. F. Carroll, O. Jeon, E. Alsberg, P. A. J. Brama and D. J. Kelly, *Acta Biomater.*, 2020, **113**, 130–143.
50 Y. Zhou, R. Qin, T. Chen, K. B. Zhang and J. C. Gui, *Mater. Des.*, 2021, **203**, 109621.
51 M. Lafuente-Merchan, S. Ruiz-Alonso, A. Zabala, P. Galvez-Martin, J. A. Marchal, B. Vazquez-Lasa, I. Gallego, L. Saenz-del-Burgo and J. L. Pedraz, *Macromol. Biosci.*, 2022, **22**, 2100435.
52 A. Sadeghianmaryan, S. Naghieh, Z. Yazdanpanah, H. A. Sardroud, N. K. Sharma, L. D. Wilson and X. B. Chen, *Int. J. Biol. Macromol.*, 2022, **204**, 62–75.
53 P. Chen, L. Cui, G. F. Chen, T. You, W. Li, J. W. Zuo, C. Wang, W. T. Zhang and C. Q. Jiang, *Int. J. Biol. Macromol.*, 2019, **138**, 79–88.
54 Z. Yang, T. Y. Zhao, C. J. Gao, F. Y. Cao, H. Li, Z. Y. Liao, L. W. Fu, P. X. Li, W. Chen, Z. Q. Sun, S. P. Jiang, Z. Tian, G. Z. Tian, K. K. Zha, T. T. Pan, X. Li, X. Sui, Z. G. Yuan, S. Y. Liu and Q. Y. Guo, *ACS Appl. Mater. Interfaces*, 2021, **13**, 23369–23383.
55 B. A. G. de Melo, Y. A. Jodat, S. Mehrotra, M. A. Calabrese, T. Kamperman, B. B. Mandal, M. H. A. Santana, E. Alsberg, J. Leijten and S. R. Shin, *Adv. Funct. Mater.*, 2019, **29**, 1906330.
56 R. Akman, H. Ramaraju and S. J. Hollister, *Adv. Eng. Mater.*, 2021, **23**, 2100219.
57 K.-C. Hung, C.-S. Tseng, L.-G. Dai and S.-H. Hsu, *Biomaterials*, 2016, **83**, 156–168.
58 Y.-T. Wen, N.-T. Dai and S.-H. Hsu, *Acta Biomater.*, 2019, **88**, 301–313.
59 N. J. Castro, J. O'Brien and L. G. Zhang, *Nanoscale*, 2015, **7**, 14010–14022.
60 Y. T. Huang, X. L. Meng, Z. Zhou, W. X. Zhu, X. Chen, Y. H. He, N. He, X. X. Han, D. M. Zhou, X. C. Duan, P. M. Vadgama and H. R. Liu, *J. Mater. Chem. B*, 2022, **10**, 7030–7044.
61 T. Brossier, G. Volpi, J. Vasquez-Villegas, N. Petitjean, O. Guillaume, V. Lapinte and S. Blanquer, *Biomacromolecules*, 2021, **22**, 3873–3883.
62 Y. Y. Du, H. M. Liu, Q. Yang, S. Wang, J. L. Wang, J. Ma, I. Noh, A. G. Mikos and S. M. Zhang, *Biomaterials*, 2017, **137**, 37–48.
63 X. Gu, Y. Zha, Y. W. Li, J. Chen, S. B. Liu, Y. Y. Du, S. M. Zhang and J. L. Wang, *Acta Biomater.*, 2022, **141**, 190–197.
64 D. H. Rosenzweig, E. Carelli, T. Steffen, P. Jarzem and L. Haglund, *Int. J. Mol. Sci.*, 2015, **16**, 15118–15135.
65 P. Zare, M. Pezeshki-Modaress and S. M. Davachi, *et al.*, An additive manufacturing-based 3D printed poly ε-caprolactone/alginate sulfate/extracellular matrix construct for nasal cartilage regeneration, *J. Biomed. Mater.*

 

*Res.*, 2022, **110**(6), 1199–1209, DOI: 10.1002/jbm.a.37363; P. Zare, M. Pezeshki-Modaress, S. M. Davachi, H. Chahsetareh, S. Simorgh, N. Asgari, M. A. Haramshahi, R. Alizadeh, Z. Bagher and M. Farhadi, *J. Biomed. Mater. Res. Part A*, 2022, **110**, 1199–1209.

66 P. R. Wei, Y. Xu, H. K. Zhang and L. M. Wang, *Chem. Eng. J.*, 2021, **422**, 130051.

67 K. Thunsiri, S. Pitjamit, P. Pothacharoen, D. Pruksakorn, W. Nakkiew and W. Wattanutchariya, *Materials*, 2020, **13**, 3417.

68 C. Mota, D. Puppi, F. Chiellini and E. Chiellini, *J. Tissue Eng. Regener. Med.*, 2015, **9**, 174–190.

69 A. Zaszczynska, M. Moczulska-Heljak, A. Gradys and P. Sajkiewicz, *Materials*, 2021, **14**, 3149.

70 M. Saadi, A. Maguire, N. T. Pottackal, M. S. H. Thakur, M. M. Ikram, A. J. Hart, P. M. Ajayan and M. M. Rahman, *Adv. Mater.*, 2022, **34**, 2108855.

71 J. A. Lewis, *Adv. Funct. Mater.*, 2006, **16**, 2193–2204.

72 A. K. Miri, D. Nieto, L. Iglesias, H. Goodarzi Hosseinabadi, S. Maharjan, G. U. Ruiz-Esparza, P. Khoshakhlagh, A. Manbachi, M. R. Dokmeci, S. C. Chen, S. R. Shin, Y. S. Zhang and A. Khademhosseini, *Adv. Mater.*, 2018, **30**, 1800242.

73 S. Q. Wang, S. Zhao, J. C. Yu, Z. Gu and Y. Q. Zhang, *Small*, 2022, **18**, 2201869.

74 J. Creff, R. Courson, T. Mangeat, J. Foncy, S. Souleille, C. Thibault, A. Besson and L. Malaquin, *Biomaterials*, 2019, **221**, 119404.

75 Z. Wang, R. Abdulla, B. Parker, R. Samanipour, S. Ghosh and K. Kim, *Biofabrication*, 2015, **7**, 045009.

76 C. Mandrycky, Z. Wang, K. Kim and D.-H. Kim, *Biotechnol. Adv.*, 2016, **34**, 422–434.

77 A. V. Gusarov, T. Laoui, L. Froyen and V. I. Titov, *Int. J. Heat Mass Transfer*, 2003, **46**, 1103–1109.

78 A. Mazzoli, *Med. Biol. Eng. Comput.*, 2013, **51**, 245–256.

79 M. Kandis and T. L. Bergman, *J. Eng. Ind.*, 2000, **122**, 439–444.

80 G. L. Ying, N. Jiang, S. Mahar, Y. X. Yin, R. R. Chai, X. Cao, J. Z. Yang, A. K. Miri, S. Hassan and Y. S. Zhang, *Adv. Mater.*, 2018, **30**, 1805460.

81 G. Tan, J. Xu, Q. Yu, J. Y. Zhang, X. F. Hu, C. W. Sun and H. Zhang, *Micromachines*, 2022, **13**, 1038.

82 Z. X. Li, X. Zhang, T. Yuan, Y. Zhang, C. Y. Luo, J. Y. Zhang, Y. Liu and W. M. Fan, *Tissue Eng., Part A*, 2020, **26**, 886–895.

83 H. Lin, A. M. Beck, K. Shimomura, J. Sohn, M. R. Fritch, Y. H. Deng, E. J. Kilroy, Y. Tang, P. G. Alexander and R. S. Tuan, *J. Tissue Eng. Regener. Med.*, 2019, **13**, 1418–1429.

84 H. Mittal, S. S. Ray, B. S. Kaith, J. K. Bhatia, Sukriti, J. Sharma and S. M. Alhassan, *Eur. Polym. J.*, 2018, **109**, 402–434.

85 S. Young, M. Wong, Y. Tabata and A. G. Mikos, *J. Controlled Release*, 2005, **109**, 256–274.

86 J. Y. Lai and Y. T. Li, *Biomacromolecules*, 2010, **11**, 1387–1397.

87 J. H. Huang, Z. W. Huang, Y. J. Liang, W. H. Yuan, L. M. Bian, L. Duan, Z. B. Rong, J. Y. Xiong, D. P. Wang and J. Xia, *Biomater. Sci.*, 2021, **9**, 2620–2630.

88 K. E. Yu, K. D. Alder, M. T. Morris, A. M. Munger, I. Lee, S. V. Cahill, H. K. Kwon, J. Back and F. Y. Lee, *Ther. Adv. Musculoskeletal Dis.*, 2020, **12**, 1759720X20966135.

89 C. Ye, J. Chen, Y. Qu, H. Qi, Q. Wang, Z. Yang, A. Wu, F. Wang and P. Li, *J. Orthop. Transl.*, 2022, **32**, 1–11.

90 Z. Y. Zhou, J. Cui, S. L. Wu, Z. Geng and J. C. Su, *Theranostics*, 2022, **12**, 5103–5124.

91 Y. Kambe, *Polym. J.*, 2021, **53**, 1345–1351.

92 W. Shi, M. Sun, X. Hu, B. Ren, J. Cheng, C. Li, X. Duan, X. Fu, J. Zhang, H. Chen and Y. Ao, *Adv. Mater.*, 2017, **29**, 1701089.

93 V. Ravichandran and A. Jayakrishnan, *Int. J. Biol. Macromol.*, 2018, **108**, 1101–1109.

94 S. A. Baeurle, M. G. Kiselev, E. S. Makarova and E. A. Nogovitsin, *Polymer*, 2009, **50**, 1805–1813.

95 Y. Z. Jiang and R. S. Tuan, *Nat. Rev. Rheumatol.*, 2015, **11**, 206–212.

96 B. Velasco-Rodriguez, T. Diaz-Vidal, L. C. Rosales-Rivera, C. A. Garcia-Gonzalez, C. Alvarez-Lorenzo, A. Al-Modlej, V. Dominguez-Arca, G. Prieto, S. Barbosa, J. Martinez and P. Taboada, *Int. J. Mol. Sci.*, 2021, **22**, 6758.

97 B. Grigolo, L. Roseti, M. Fiorini, M. Fini, G. Giavaresi, N. N. Aldini, R. Giardino and A. Facchini, *Biomaterials*, 2001, **22**, 2417–2424.

98 M. Bishnoi, A. Jain, P. Hurkat and S. Jain, *Glycoconjugate J.*, 2016, **33**, 693.

99 P. Agrawal, K. Pramanik, V. Vishwanath, A. Biswas, A. Bissoyi and P. K. Patra, *J. Biomed. Mater. Res., Part B*, 2018, **106**, 2576.

100 J. H. Elisseeff, S. Fermanian, D. Wang, B. Sharma, S. Varghese, D. H. Fairbrother, I. Strehin, J. Gorham and B. Cascio, *Nat. Mater.*, 2007, **6**, 385.

101 C. B. Foldager, C. Bünger, A. B. Nielsen, M. Ulrich-Vinther, S. Munir, H. Everland and M. Lind, *Int. Orthop.*, 2012, **36**, 1507.

102 J. Valcarcel, R. Novoa-Carballal, R. I. Pérez-Martín, R. L. Reis and J. A. Vázquez, *Biotechnol. Adv.*, 2017, **35**, 711.

103 B. E. Uygun, S. E. Stojsih and H. W. T. Matthew, *Tissue Eng., Part A*, 2009, **15**, 3499.

104 J. K. F. Suh and H. W. T. Matthew, *Biomaterials*, 2000, **21**, 2589.

105 H. J. Huang, X. Zhang, X. Q. Hu, Z. X. Shao, J. X. Zhu, L. H. Dai, Z. T. Man, L. Yuan, H. F. Chen, C. Y. Zhou and Y. F. Ao, *Biomaterials*, 2014, **35**, 9608–9619.

106 E. Tamjid, M. Bohlouli, S. Mohammadi, H. Alipour and M. Nikkhah, *J. Biomed. Mater. Res., Part A*, 2020, **108**, 1426–1438.

107 Y. B. Zhang, X. C. Liu, L. D. Zeng, J. Zhang, J. L. Zuo, J. Zou, J. X. Ding and X. S. Chen, *Adv. Funct. Mater.*, 2019, **29**, 1903279.

108 K. Budak, O. Sogut and U. A. Sezer, *J. Polym. Res.*, 2020, **27**, 1–19.

109 P. Zare, M. Pezeshki-Modaress, S. M. Davachi, P. Zare, F. Yazdian, S. Simorgh, H. Ghanbari, H. Rashedi and Z. Bagher, *Carbohydr. Polym.*, 2021, **266**, 118123.

110 G. H. Zhen, Q. Y. Guo, Y. S. Li, C. L. Wu, S. A. Zhu, R. M. Wang, X. E. Guo, B. C. Kim, J. Huang, Y. Z. Hu,

Y. Dan, M. Wan, T. Ha, S. An and X. Cao, *Nat. Commun.*, 2021, **12**, 1706.
111 X. Zhou, T. Esworthy, S. J. Lee, S. Miao, H. T. Cui, M. Plesiniak, H. Fenniri, T. Webster, R. D. Rao and L. G. Zhang, *Nanomedicine*, 2019, **19**, 58–70.
112 A. V. Salvekar, Y. Zhou, W. M. Huang, Y. S. Wong, S. S. Venkatraman, Z. X. Shen, G. M. Zhu and H. P. Cui, *Eur. Polym. J.*, 2015, **72**, 282–295.
113 H. F. Sun, L. Mei, C. X. Song, X. M. Cui and P. Y. Wang, *Biomaterials*, 2006, **27**, 1735–1740.
114 G. H. Zhen and X. Cao, *Trends Pharmacol. Sci.*, 2014, **35**, 227–236.
115 J. Y. Liu, L. Li, H. R. Suo, M. L. Yan, J. Yin and J. Z. Fu, *Mater. Des.*, 2019, **171**, 107708.
116 C. J. Shuai, C. D. Gao, Y. Nie, H. L. Hu, Y. Zhou and S. P. Peng, *Nanotechnology*, 2011, **22**, 285703.
117 N. Fu, J. F. Liao, S. Y. Lin, K. Sun, T. R. Tian, B. F. Zhu and Y. F. Lin, *Cell Proliferation*, 2016, **49**, 729–739.
118 M. C. Vyner, A. N. Li and B. G. Amsden, *Biomaterials*, 2014, **35**, 9041–9048.
119 A. Asti and L. Gioglio, *Int. J. Artif. Organs*, 2014, **37**, 187–205.
120 Z. Liu, Y. Xu, L. Cao, C. Bao, H. Sun, L. Wang, K. Dai and L. Zhu, *Soft Matter*, 2012, **8**, 5888–5895.
121 S. Sartori, V. Chiono, C. Tonda-Turo, C. Mattu and C. Gianluca, *J. Mater. Chem. B*, 2014, **2**, 5128–5144.
122 K.-C. Hung, C.-S. Tseng, L.-G. Dai and S.-H. Hsu, *Biomaterials*, 2016, **83**, 156–168.
123 W. Xu, X. H. Wang, Y. N. Yan and R. J. Zhang, *J. Bioact. Compat. Polym.*, 2008, **23**, 103–114.
124 Y. Huang, K. He and X. Wang, *Mater. Sci. Eng., C*, 2013, **33**, 3220–3229.
125 E. Zeimaran, S. Pourshahrestani, B. Pingguan-Murphy, D. Kong, S. V. Naveen, T. Kamarul and N. A. Kadri, *Carbohydr. Polym.*, 2017, **175**, 618–627.
126 D. Lin, B. Cai, L. Wang, L. Cai, Z. Wang, J. Xie, Q.-X. Lv, Y. Yuan, C. Liu and S. G. F. Shen, *Biomaterials*, 2021, **269**, 120095.
127 A. Barkane, O. Platnieks, M. Jurinovs and S. Gaidukovs, *Polym. Degrad. Stab.*, 2020, **181**, 109347.
128 J. Yang, A. R. Webb, S. J. Pickerill, G. Hageman and G. A. Ameer, *Biomaterials*, 2006, **27**, 1889–1898.
129 Y. Li, G. A. Thouas and Q.-Z. Chen, *RSC Adv.*, 2012, **2**, 8229–8242.
130 S. Pourshahrestani, E. Zeimaran, N. A. Kadri, N. Gargiulo, H. M. Jindal, K. Hasikin, S. V. Naveen, S. D. Sekaran and T. Kamarul, *Mater. Sci. Eng., C*, 2019, **98**, 1022–1033.
131 A. K. Sharma, P. V. Hota, D. J. Matoka, N. J. Fuller, D. Jandali, H. Thaker, G. A. Ameer and E. Y. Cheng, *Biomaterials*, 2010, **31**, 6207–6217.
132 E. J. Chung, H. Qiu, P. Kodali, S. Yang, S. M. Sprague, J. Hwong, J. Koh and G. A. Ameer, *J. Biomed. Mater. Res., Part A*, 2011, **96A**, 29–37.
133 L. Vogt, F. Ruther, S. Salehi and A. R. Boccaccini, *Adv. Healthcare Mater.*, 2021, **10**, 2002026.
134 S. Salehi, M. Czugala, P. Stafiej, M. Fathi, T. Bahners, J. S. Gutmann, B. B. Singer and T. A. Fuchsluger, *Acta Biomater.*, 2017, **50**, 370–380.
135 H. Ramaraju, L. D. Solorio, M. L. Bocks and S. J. Hollister, *PLoS One*, 2020, **15**, e0229112.
136 F. Migneco, Y. C. Huang, R. K. Birla and S. J. Hollister, *Biomaterials*, 2009, **30**, 6479.
137 L. D. Solorio, M. L. Bocks and S. J. Hollister, *J. Biomed. Mater. Res., Part A*, 2017, **105**, 1618.
138 D. S. Branciforti, S. Lazzaroni, C. Milanese, M. Castiglioni, F. Auricchio, D. Pasini and D. Dondi, *Addit. Manuf.*, 2019, **25**, 317–324.
139 S. M. Danov, O. A. Kazantsev, A. L. Esipovich, A. S. Belousov, A. E. Rogozhin and E. A. Kanakov, *Catal. Sci. Technol.*, 2017, **7**, 3659–3675.
140 J. Stampfl, M. Schuster, S. Baudis, H. Lichtenegger, R. Liska, C. Turecek and E. Varga, Biodegradable stereolithography resins with defined mechanical properties, Leiria, Portugal, 2007.
141 X. L. Niu, N. Li, Z. P. Du and X. M. Li, *Bioact. Mater.*, 2023, **20**, 574–597.
142 Y. Krishnan and A. J. Grodzinsky, *Matrix Biol.*, 2018, **71–72**, 51–69.
143 R. Shi, Y. Huang, C. Ma, C. Wu and W. Tian, *Front. Med.*, 2019, **13**, 160–188.
144 P. Sharma, P. Kumar, R. Sharma, V. D. Bhatt and P. S. Dhot, *J. Med. Life*, 2019, **12**, 225–229.
145 X. J. Liu, H. Y. Meng, Q. Y. Guo, B. C. Sun, K. H. Zhang, W. Yu, S. C. Liu, Y. Wang, X. G. Jing, Z. Z. Zhang, J. Peng and J. H. Yang, *Cell Tissue Res.*, 2018, **372**, 13–22.
146 X. D. Tang, H. Muhammad, C. McLean, J. Miotla-Zarebska, J. Fleming, A. Didangelos, P. Onnerfjord, A. Leask, J. Saklatvala and T. L. Vincent, *Ann. Rheum. Dis.*, 2018, **77**, 1372–1380.
147 J. Crecente-Campo, E. Borrajo, A. Vidal and M. Garcia-Fuentes, *Eur. J. Pharm. Biopharm.*, 2017, **114**, 69–78.
148 W. Y. Yang, Y. T. Cao, Z. Zhang, F. C. Du, Y. P. Shi, X. M. Li and Q. Q. Zhang, *Acta Biomater.*, 2018, **69**, 170–182.
149 L. Geary and C. LaBonne, *eLife*, 2018, **7**, e33845.
150 S. Lu, J. Lam, J. E. Trachtenberg, E. J. Lee, H. Seyednejad, J. van den Beucken, Y. Tabata, M. E. Wong, J. A. Jansen, A. G. Mikos and F. K. Kasper, *Biomaterials*, 2014, **35**, 8829–8839.
151 M. K. Boushell, C. Z. Mosher, G. K. Suri, S. B. Doty, E. J. Strauss, E. B. Hunziker and H. H. Lu, *Ann. N. Y. Acad. Sci.*, 2019, **1442**, 138–152.
152 Y. H. Lee, H. C. Wu, C. W. Yeh, C. H. Kuan, H. T. Liao, H. C. Hsu, J. C. Tsai, J. S. Sun and T. W. Wang, *Acta Biomater.*, 2017, **63**, 210–226.
153 C. R. Rowland, K. A. Glass, A. R. Ettyreddy, C. C. Gloss, J. R. L. Matthews, N. P. T. Huynh and F. Guilak, *Biomaterials*, 2018, **177**, 161–175.
154 T. Gonzalez-Fernandez, S. Rathan, C. Hobbs, P. Pitacco, F. E. Freeman, G. M. Cunniffe, N. J. Dunne, H. O. McCarthy, V. Nicolosi, F. J. O'Brien and D. J. Kelly, *J. Controlled Release*, 2019, **301**, 13–27.

155 H. Madry, L. Gao, A. Rey-Rico, J. K. Venkatesan, K. Muller-Brandt, X. Y. Cai, L. Goebel, G. Schmitt, S. Speicher-Mentges, D. Zurakowski, M. D. Menger, M. W. Laschke and M. Cucchiarini, *Adv. Mater.*, 2020, **32**, 1906508.
156 M. Zanatta, M. T. Valenti, L. Donatelli, C. Zucal and L. D. Carbonare, *J. Bone Miner. Metab.*, 2012, **30**, 706–714.
157 R. M. Stefani, A. J. Lee, A. R. Tan, S. S. Halder, Y. Z. Hu, X. E. Guo, A. M. Stoker, G. A. Ateshian, K. G. Marra, J. L. Cook and C. T. Hung, *Acta Biomater.*, 2020, **102**, 326–340.
158 K. C. Hung, C. S. Tseng, L. G. Dai and S. H. Hsu, *Biomaterials*, 2016, **83**, 156–168.
159 Y. Sato, H. Mera, D. Takahashi, T. Majima, N. Iwasaki, S. Wakitani and M. Takagi, *Cytotechnology*, 2017, **69**, 405–416.
160 P. F. Hu, W. P. Chen, J. L. Tang, J. P. Bao and L. D. Wu, *Phytother. Res.*, 2011, **25**, 878–885.
161 T. Li, B. Z. Liu, K. Chen, Y. Y. Lou, Y. H. Jiang and D. Zhang, *Biomed. Pharmacother.*, 2020, **131**, 110652.
162 M. K. Kim, H. Y. Lee, K. S. Park, E. H. Shin, S. H. Jo, J. Yun, S. W. Lee, Y. H. Yoo, Y. S. Lee, S. H. Baek and Y. S. Bae, *Biochem. Pharmacol.*, 2005, **70**, 1764–1771.
163 W. X. Zhu, Z. Zhou, Y. T. Huang, H. R. Liu, N. He, X. L. Zhu, X. X. Han, D. M. Zhou, X. C. Duan, X. Chen, Y. H. He, X. L. Meng and S. Zhu, *J. Mater. Sci. Technol.*, 2023, **136**, 200–211.
164 Y. Li, C. Jiang, D. Zhang, Y. Wang, X. Ren, K. Ai, X. Chen and L. Lu, *Acta Biomater.*, 2017, **47**, 124–134.
165 X. Chen, R. Tong, B. Liu, H. Liu, X. Feng, S. Ding, Q. Lei, G. Tang, J. Wu and W. Fang, *Biomater. Sci.*, 2019, **8**, 1380–1393.
166 X. Deng, S. Liang, X. Cai, S. Huang, Z. Cheng, Y. Shi, M. Pang, P. Ma and J. Lin, *Nano Lett.*, 2019, **19**, 6772–6780.
167 Y. Wan, J. Fang, Y. Wang, J. Sun, Y. Sun, X. Sun, M. Qi, W. Li, C. Li, Y. Zhou, L. Xu, B. Dong and L. Wang, *Adv. Healthcare Mater.*, 2021, **10**, 101515.
168 F. J. O'Brien, *Mater. Today*, 2011, **14**, 88–95.
169 B. Balakrishnan and R. Banerjee, *Chem. Rev.*, 2011, **111**, 4453–4474.
170 J. N. Fu, X. Wang, M. Yang, Y. R. Chen, J. Y. Zhang, R. H. Deng, Z. N. Zhang, J. K. Yu and F. Z. Yuan, *Front. Bioeng. Biotechnol.*, 2021, **9**, 812383.
171 S. E. El-Habashy, H. M. Eltaher, A. Gaballah, E. I. Zaki, R. A. Mehanna and A. H. El-Kamel, *Mater. Sci. Eng., C*, 2021, **119**, 111599.
172 N. T. Khanarian, N. M. Haney, R. A. Burga and H. H. Lu, *Biomaterials*, 2012, **33**, 5247–5258.
173 S. A. Zhu, P. F. Chen, Y. Chen, M. Z. Li, C. Chen and H. B. Lu, *Am. J. Sports Med.*, 2020, **48**, 2808–2818.
174 C. H. Chang, F. H. Lin, C. C. Lin, C. H. Chou and H. C. Liu, Cartilage tissue engineering on the surface of a novel gelatin-calcium-phosphate biphasic scaffold in a double-chamber bioreactor, *J. Biomed. Mater. Res. B Appl. Biomater.*, 2004, **71**, 313–321; C. H. Chang, F. H. Lin, C. C. Lin, C. H. Chou and H. C. Liu, *J. Biomed. Mater. Res. B Appl. Biomater.*, 2004, **71B**, 313–321.
175 S.-J. Seo, C. Mahapatra, R. K. Singh, J. C. Knowles and H.-W. Kim, *J. Tissue Eng.*, 2014, **5**, 2041731414541850.
176 T. J. Levingstone, A. Matsiko, G. R. Dickson, F. J. O'Brien and J. P. Gleeson, *Acta Biomater.*, 2014, **10**, 1996–2004.
177 Z. Y. Li, S. J. Jia, Z. Xiong, Q. F. Long, S. R. Yan, F. Hao, J. Liu and Z. Yuan, *J. Biosci. Bioeng.*, 2018, **126**, 389–396.
178 B. Zhang, J. Huang and R. J. Narayan, *J. Mater. Chem. B*, 2020, **8**, 8149–8170.
179 Y. Sun, Y. Q. You, W. B. Jiang, B. Wang, Q. Wu and K. R. Dai, *Sci. Adv.*, 2020, **6**, 1422.
180 P. Nooeaid, V. Salih, J. P. Beier and A. R. Boccaccini, *J. Cell. Mol. Med.*, 2012, **16**, 2247–2270.
181 P. Nooeaid, J. A. Roether, E. Weber, D. W. Schubert and A. R. Boccaccini, Technologies for multilayered scaffolds suitable for interface tissue engineering, *Adv. Eng. Mater.*, 2014, **16**, 319–327; P. Nooeaid, J. A. Roether, E. Weber, D. W. Schubert and A. R. Boccaccini, *Adv. Eng. Mater.*, 2014, **16**, 319–327.
182 J. L. Xu, J. D. Ji, J. Y. Jiao, L. J. Zheng, Q. M. Hong, H. Z. Tang, S. T. Zhang, X. H. Qu and B. Yue, *Front. Bioeng. Biotechnol.*, 2022, **10**, 828921.
183 C. C. Li, L. L. Ouyang, I. J. Pence, A. C. Moore, Y. Y. Lin, C. W. Winter, J. P. K. Armstrong and M. M. Stevens, *Adv. Mater.*, 2019, **31**, 1900291.
184 C. C. Li, J. P. K. Armstrong, I. J. Pence, W. Kit-Anan, J. L. Puetzer, S. C. Carreira, A. C. Moore and M. M. Stevens, *Biomaterials*, 2018, **176**, 24–33.
185 X. L. Niu, N. Li, Z. P. Du and X. M. Li, *Bioact. Mater.*, 2023, **20**, 574–597.
186 B. P. Chan and K. W. Leong, *Eur. Spine J.*, 2008, **17**, S467–S479.
187 V. Karageorgiou and D. Kaplan, *Biomaterials*, 2005, **26**, 5474–5491.
188 M. A. Velasco, C. A. Narvaez-Tovar and D. A. Garzon-Alvarado, *BioMed Res. Int.*, 2015, **2015**, 729076.
189 R. A. Perez and G. Mestres, *Mater. Sci. Eng., C*, 2016, **61**, 922–939.
190 S. I. Roohani-Esfahani, P. Newman and H. Zreiqat, *Sci. Rep.*, 2016, **6**, 19468.
191 D. W. Hutmacher, *Biomaterials*, 2000, **21**, 2529–2543.
192 P. Lee, K. Tran, W. Chang, Y. L. Fang, G. Zhou, R. Junka, N. B. Shelke, X. J. Yu and S. G. Kumbar, *Polym. Adv. Technol.*, 2015, **26**, 1476–1485.
193 Y. Shanjani, C. C. Pan, L. Elomaa and Y. Yang, *Biofabrication*, 2015, **7**, 045008.
194 A. Di Luca, B. Ostrowska, I. Lorenzo-Moldero, A. Lepedda, W. Swieszkowski, C. Van Blitterswijk and L. Moroni, *Sci. Rep.*, 2016, **6**, 22898.
195 A. Ergun, X. J. Yu, A. Valdevit, A. Ritter and D. M. Kalyon, *Tissue Eng., Part A*, 2012, **18**, 2426–2436.
196 S. M. Bittner, B. T. Smith, L. Diaz-Gomez, C. D. Hudgins, A. J. Melchiorri, D. W. Scott, J. P. Fisher and A. G. Mikos, *Acta Biomater.*, 2019, **90**, 37–48.
197 D. J. Huey, J. C. Hu and K. A. Athanasiou, *Science*, 2012, **338**, 917–921.